TABLE 2
Primer used for cloning

Number	Oligonucleotide sequence[a]	Forward/Reverse	Enzyme site	Description	Type
1	ACGT**CTCGAG**GCCTCGCAGCGGTGACGAG	Reverse	XhoI	Reverse primer	Normal, in/del
2	ACGT**GAGCTC**AGATGCAGCCCAATCTTCTCCTAACA	Forward	SacI	Normal or in/del: full-length	Normal, in/del
3	ACGT**GAGCTC**CCCCTCCTTTCTCTCCCGGGTG	Forward	SacI	Normal or in/del: Δ82	Normal, in/del
4	ACGT**GAGCTC**TGTCTAGCAGTGTCTACCCTGTGGCA	Forward	SacI	Normal: Δ298	Normal
5	ACGT**GAGCTC**GGTGTACCTGCTGTTAAAGGAGGT	Forward	SacI	Normal: Δ384	Normal
6	ACGT**GAGCTC**AATGGGTGAGTAGGGATGGATTACA	Forward	SacI	Normal: Δ543	Normal
7	ACGT**GAGCTC**AATGGGTGAGTAGGGATGGATTA	Forward	SacI	In/del: Δ148	In/del
8	AATGGGTGAGTAGGGATGGATTACACC	Inverse-F		In/del: Δin/del-F	In/del
9	CCGGGAGAGAAAGGAGGGCAA	Inverse-R		In/del: Δin/del-R	In/del

[a] Boldface sequence, restriction enzyme site for cloning.

TABLE 3
EMSA probe sequence

Number	Type	Probe sequence
1	Sense	AGATGCAGCCCAATCTTCTCCTAACATCTGGATTCCTCTC
	Antisense	GAGAGGAATCCAGATGTTAGGAGAAGATTGGGCTGCATCT
2	Sense	GATTCCTCTCTGTCACTGCATTCCCTCCTGTCATCCTGCC
	Antisense	GGCAGGATGACAGGAGGGAATGCAGTGACAGAGAGGAATC
3	Sense	TCATCCTGCCTTTGTTTTCTTGCCCTCCTTTCTCTCCCGG
	Antisense	CCGGGAGAGAAAGGAGGGCAAGAAAACAAAGGCAGGATGA
4	Sense	GGTGTACCTGCTGTTAAAGGAGGTTACGACCTCTGATGCT
	Antisense	AGCATCAGAGGTCGTAACCTCCTTTAACAGCAGGTACACC
5	Sense	ATGCTGGGGTGGCCAGAGGGGATGGGAGTGGGTCTGGCAC
	Antisense	GTGCCAGACCCACTCCCATCCCCTCTGGCCACCCCAGCAT
6	Sense	GGCACTCTGAGGAAAGGGGGTGAAACCAGCTGAGAAGTCA
	Antisense	TGACTTCTCAGCTGGTTTCACCCCCTTTCCTCAGAGTGCC
7	Sense	AGTCATCTTTTACCTGCTGGCATGGCCCCAGCCAGGGTTC
	Antisense	GAACCCTGGCTGGGGCCATGCCAGCAGGTAAAAGATGACT
8	Sense	CCCCAGCCAGGGTTCTGTTGCTATGGGAGAATGGGTGAGT
	Antisense	ACTCACCCATTCTCCCATAGCAACAGAACCCTGGCTGGGG
9	Sense	TCTCTCCCGGTTATTAATTAATTAACTAAAATTAAATTAT
	Antisense	ATAATTTAATTTTAGTTAATTAATTAATAACCGGGAGAGA
10	Sense	AATTATTTAGTTAATTTAATTAACTAAACTAATGGGTGAG
	Antisense	CTCACCCATTAGTTTAGTTAATTAAATTAACTAAATAATT

of heparinized blood over a Ficoll-Paque PREMIUM (GE Healthcare) gradient, according to the manufacturer's instructions. The peripheral blood mononuclear cells were then cultured at 37 °C in 5% CO_2 with plate-bound anti-CD3 monoclonal antibodies (BD Pharmingen) in GT-T502 medium (Kohjin Bio, Sakado, Japan) supplemented with recombinant interleukin-2 (IL-2) at 175 Japan reference units/ml. After 5 days, activated peripheral blood mononuclear cells were collected and transferred to 6-well plates (1.5×10^6 cells/well) coated with anti-CD3 monoclonal antibodies, and the cells were incubated for an additional 24 h. A solution containing Sendai virus vectors that individually carried OCT3/4, SOX2, KLF4, and c-MYC (DNAVEC Inc., Japan) was added to each well. At 24 h postinfection, the medium was changed to fresh CT-T502 medium. At 48 h postinfection, the cells were collected and transferred to a 10-cm dish that contained mitomycin C-inactivated mouse embryonic fibroblast feeder cells (6×10^4 to 6×10^5 cells/dish). After an additional 24 h of incubation, the medium was changed to iPSC medium, which consisted of DMEM/F-12 medium (Sigma) supplemented with 20% knockout serum replacement (Invitrogen), 1 mM L-glutamine, 1 mM non-essential amino acids, 0.1 mM β-mercaptoethanol, 50 units of penicillin, 50 mg/ml streptomycin, and 4 ng/ml basic fibroblast growth factor (Wako Pure Chemical Industries, Osaka, Japan). The iPSC medium was changed every other day until colonies were picked. The generated iPSCs were maintained on irradiated mouse embryonic fibroblast feeder cells in iPSC medium. Culture medium for the iPSCs was changed every 2 days, and the cells were passaged using 1 mg/ml collagenase IV every 5–6 days.

EMSA—Nuclear extracts were prepared with a CelLytic nuclear extraction kit (Sigma), according to the manufacturer's protocol. The nuclear protein concentration of each sample was determined using a BCA protein assay kit (Thermo Scientific).

EMSA probes were 40 bp in length and are listed in Table 3. Probes 1–3 were designed to cover non-insertion/deletion and insertion/deletion regions (non-insertion/deletion, bp −4320 to −4220; insertion/deletion, bp −3936 to −3836). Probes 4–8 were designed to cover the non-insertion/deletion regulatory region (non-insertion/deletion, bp −3936 to −3777). Probes 9 and 10 were designed to cover the insertion/deletion region (insertion/deletion, −3836 to −3782 bp). Double-stranded DNA probes were biotin-labeled using a LightShift chemiluminescent EMSA kit (Thermo Scientific) and then were mixed with nuclear extracts. After 20 min, the samples were subjected to electrophoresis on 7% EMSA gels. After electrophoresis, the samples were transferred onto Biodyne B precut modified nylon membranes (Thermo Scientific). The membranes were cross-linked in a UV transilluminator for 15 min and then were incubated with blocking buffer and streptavidin-horseradish peroxidase conjugates. Bound conjugates were detected using a molecular imager (ChemiDoc XRS+, Bio-Rad).

RT-PCR—The iPSCs were removed from the feeder cells and were rinsed twice with PBS. Total cellular RNA was extracted with TRIzol reagent (Invitrogen), according to the manufactur-

er's instructions. RNA concentrations were determined by measuring absorption values at 260 nm/280 nm. Reverse transcription was performed using a SuperScript first strand synthesis system for RT-PCR kit (Invitrogen). Primer sequences for human *OCT3/4*, *NANOG*, *SOX2*, and *GAPDH* as well as the associated PCR detection methods were created and performed according to Seki *et al.* (21). The primers used to detect human *HTRA1* included AACTTTATCGCGGACGTGGTGGAG (forward) and TGATGGCGTCGGTCTGGATGTAGT (reverse).

Quantitative RT-PCR—Total RNA was isolated from human iPSCs with an RNeasy minikit (Qiagen, Hilden, Germany) according to the manufacturer's instructions. An aliquot of each sample was reverse-transcribed using a high capacity cDNA reverse transcription kit (Invitrogen) to obtain single-stranded cDNAs. Using an ABI STEP-One real-time PCR system (Invitrogen) with TaqMan probes for human *HTRA1*, quantitative RT-PCR was performed according to the manufacturer's instructions. All of the reactions were run in triplicate using the ΔCt method, and detection of human *GAPDH* was used as an internal control.

Liquid Chromatography-Mass Spectrometry (LC-MS/MS)—Nuclear extract of 661W cells (50 μg) was combined with 100 pmol of biotin-labeled, double-stranded DNA probes in DNAP buffer (20 mM HEPES, 80 mM KCl, 1 mM MgCl, 0.2 mM EDTA, 10% glycerol, 0.1% Triton X-100, 0.5 mM DTT). This proteins/probes mixture was incubated at 4 °C for 30 min before 50 ml of Dynabeads M280 streptavidin (Invitrogen) was added. The mixture was incubated at 4 °C for 30 min. The beads-probes-protein complex was then washed with 500 μl of DNAP buffer three times for 30 min at 4 °C. The washed complexes were mixed with 30 μl of SDS-PAGE sample buffer (Bio-Rad) and were boiled for 5 min at 100 °C. The boiled samples were quenched on ice for 5 min before being separated by 7.5% SDS-PAGE. Bands of interest were cut out of the gel and were processed for in-gel digestion for further LC-MS/MS analysis. A Thermo LTQ system (Thermo Scientific) and Scaffold 4 data analysis software (Matrix Science) were used.

Immunohistochemistry—Eyes from wild type, *HtrA1* knockout, and *HtrA1* transgenic mice (12, 16, 23) were resected and immersed in a fixative containing 4% paraformaldehyde overnight at 4 °C. The eyes were embedded in OCT compound and frozen on dry ice. Sections of the frozen eyes (10 μm) were washed with 0.1% Tween 20, PBS (PBST) prior to permeabilization with 0.3% Triton X-100, PBS for 15 min. After the sections were washed in 0.1% PBST, they were incubated with blocking solution for 1 h, followed by an overnight incubation at 4 °C with anti-rabbit HtrA1 antibodies (Abcam) in PBS, 2% BSA. The sections were washed in 0.1% PBST three times and then were incubated with Alexa Fluor 488-conjugated anti-rabbit IgG antibodies (1:1000; Invitrogen) and DAPI (Dojindo, Japan) for nuclear staining at room temperature. After 1 h, the sections were mounted with Ultramount aqueous permanent mounting medium (DakoCytomation, Glostrup, Denmark) and were analyzed using a confocal fluorescence laser microscope (LSM 700, Zeiss).

In Situ Hybridization—Eyes from *HtrA1* heterozygous mice were removed and immersed in 5% formaldehyde overnight at 4 °C. The eyes were then embedded in paraffin and sectioned (10 μm). *In situ* hybridization was performed using a QuantiGene™ ViewRNA system (Affymetrix, Santa Clara, CA) using HtrA1 and LacZ probes according to the manufacturer's instructions.

Western Blotting—Total proteins were extracted from mouse brain tissues in ice-cold TNE buffer (10 mM Tris-HCl, 100 mM NaCl, 10 mM EDTA, 0.1% Nonidet P-40) containing protease and phosphatase inhibitors (Roche Applied Science). Protein concentrations of the extracts were determined using a BCA assay kit (Thermo Scientific). Equal amounts of protein (10 μg/lane) were separated by 7.5% SDS-PAGE and were transferred to PVDF membranes (Trans-Blot Turbo, Bio-Rad). The membranes were then incubated with an anti-mouse HtrA1 antibody (1:100; Abcam) and an anti-α-tubulin antibody (1:1000; Abcam). A FluorChem Western blot imaging station (ChemiDoc XRS+, Bio-Rad) and image analysis software (Image Lab, Bio-Rad) were used to calculate and normalize the pixel value of each protein band.

RESULTS

Sequencing of ARMS2-HTRA1 Loci in Controls and AMD Patients—To determine the genomic sequence of the LD block represented by the SNP, rs10490924, in association with AMD (6, 19, 24), ~10.5 kbp of the LD block (NC_000010.10) was sequenced for 228 controls and 226 AMD patients. Two unique sequences were identified in the regulatory region of *ARMS2* and *HTRA1* (Fig. 1). A C-to-A (C/A) variant was identified in the regulatory region of *ARMS2*, −550 bp upstream of exon 1 (Fig. 1, *A* and *B*), and an insertion/deletion variant was identified immediately following the *ARMS2* exon 2 in the regulatory region of *HTRA1*, −3777 bp upstream of exon 1 (Fig. 1, *A* and *C*). Sequence variations in both transcription regulators were in complete LD with SNP rs10490924, thereby suggesting that AMD and PCV pathogenesis are directly associated with these variants.

The Effect of C/A and Insertion/Deletion Variants on ARMS2 and HTRA1 Regulatory Region Activity—To date, two hypotheses have been proposed to account for the increased risk of AMD that is observed. These involve an increase in the transcription of *HTRA1* and/or the presence of unstable *ARMS2* mRNA (7, 19, 24). To investigate the first hypothesis, regulator activity for *ARMS2* was assayed using constructs covering the regulatory region from −1,000 to +1 bp and from −600 to +1 bp. Both of these regions contain the C/A repetitive variant (Fig. 1*D*). Regulatory region activity was not detected for either the non-C/A or C/A variants of differing length for retinal cell lines (ARPE19, 661W, and RGC5 tested) (Fig. 1, *E–G*). Next, regulator activity of *HTRA1* was assayed for the −4,320 to +1 bp region of the non-insertion/deletion regulatory region and for the −3,936 to +1 bp region of the insertion/deletion regulatory region (Fig. 1*H*). Both regions had common sequences on both ends of the regulatory region. Transcription regulator activity was not found to be affected by the insertion/deletion variants in the ARPE19 cell line (Fig. 1*I*). However, activity of the insertion/deletion regulator was significantly up-regulated compared with the activity of the non-insertion/deletion regulator in both the 661W and RGC5 cell lines, by ~2- and 3-fold, respectively (Fig. 1, *J* and *K*). Moreover, *HTRA1* non-insertion/

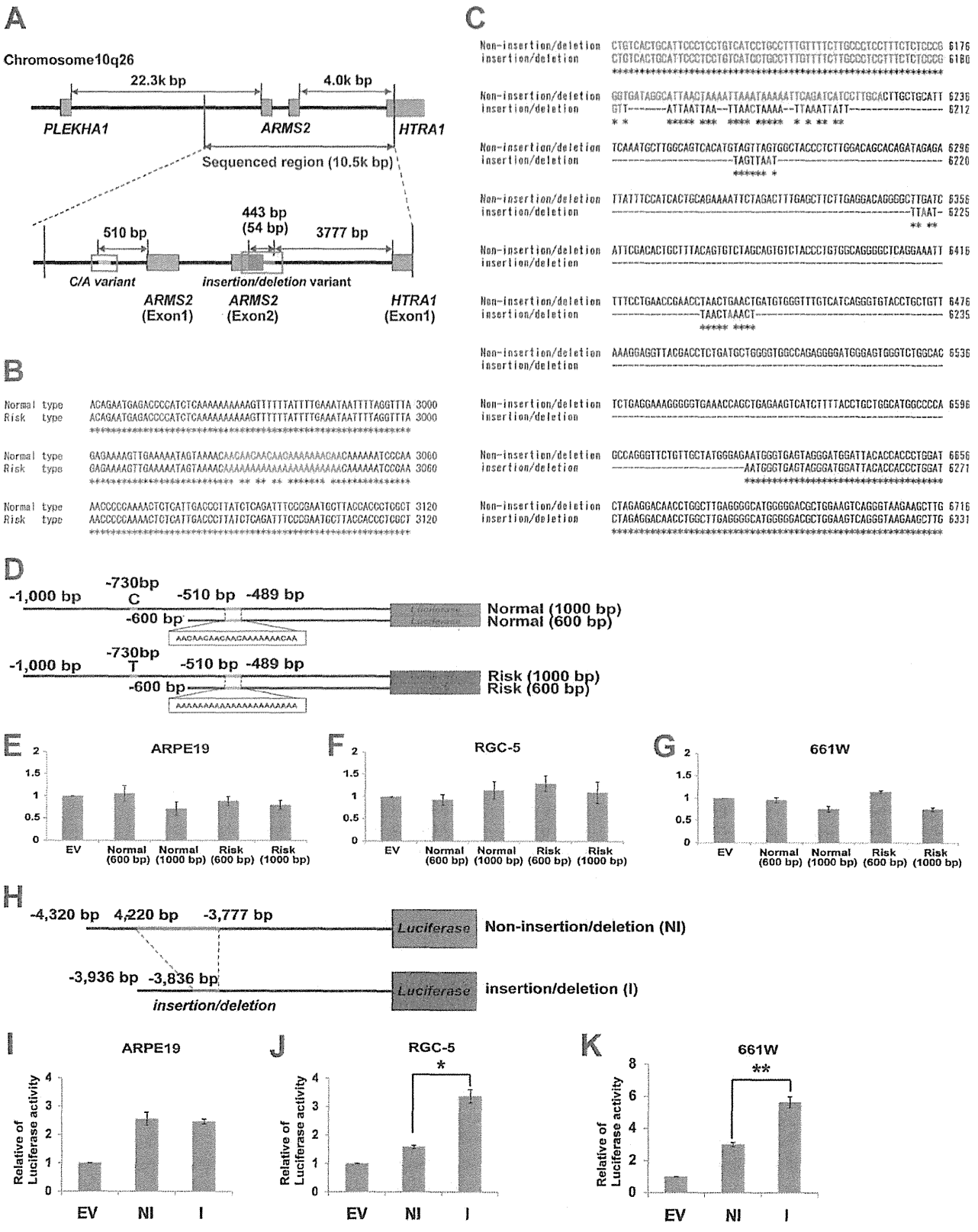

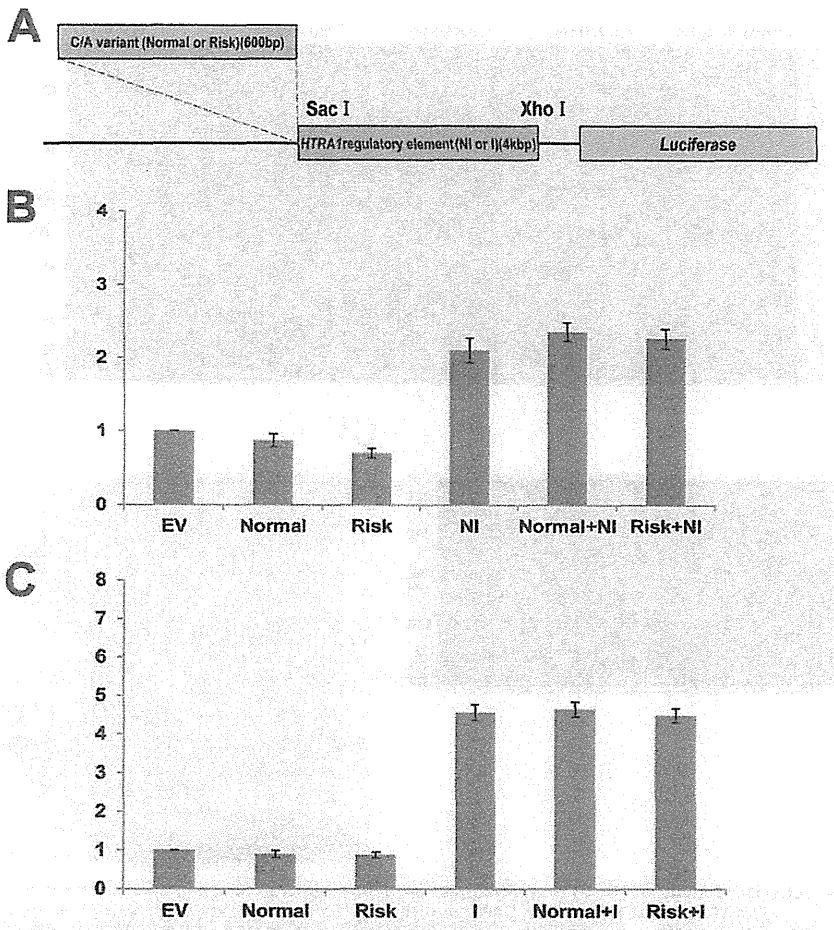

FIGURE 2. **The effect of the *ARMS2* C/A variant on the *HTRA1* transcription regulator.** *A*, schematic diagram of the C/A variant plus *HTRA1* regulatory element in the constructs used for luciferase assays (*blue region*, 600-bp *AMRS2* transcription regulatory region (contains C/A variant); *orange region*, region that contains the *HTRA1* regulatory element; *yellow region*, the luciferase reporter gene). *B*, C/A variant plus non-insertion/deletion type *HTRA1* regulatory element activity in 661W cells. *C*, C/A variant plus insertion/deletion type *HTRA1* regulatory element activity in 661W cells. *Error bars*, S.D. *EV*, empty vector; *Normal*, normal type C/A variant; *Risk*, risk type C/A variant; *NI*, non-insertion/deletion type *HTRA1* regulatory element; *I*, insertion/deletion type *HTRA1* regulatory element.

deletion regulator activity was not detected in the latter, similar to the empty vector. However, when the non-insertion/deletion regulator was replaced with the insertion/deletion regulator in the 661W and RGC5 cell lines, *HTRA1* regulatory element activity increased 2- and 3-fold, respectively (Fig. 1*J*). To test whether C/A variants in the transcription regulatory region of *ARMS2* influence *HTRA1* gene expression, both normal and risk type *ARMS2* C/A variant (Fig. 2*A*) were cloned and fused to the *HTRA1* transcription regulator of the non-insertion/deletion and insertion/deletion constructs. Luciferase levels were subsequently measured following transfection of these vectors (Fig. 2*A*). Neither the normal nor the risk type, C/A variants affected *HTRA1* transcription regulator activity (Fig. 2, *B* and *C*).

Endogenous Transcription Regulator Activity and Protein and mRNA Expression of HtrA1 in Mouse Retina Tissues—To examine the localization of HtrA1 in the retina, eye sections from both wild type and mutant (HtrA1 knock-out, HtrA1 transgenic) mice were stained with an anti-mouse HtrA1 antibody (Fig. 3*A*). In both wild type and HtrA1-Tg mouse sections,

FIGURE 1. **Transcription regulatory region of *ARMS2* and *HTRA1*.** *A*, a schematic diagram of the transcription regulatory region of *ARMS2* and *HTRA1*. Sequencing of the indicated transcription regulatory region spanned 10.5 kbp and was performed for both AMD and non-AMD controls. Two unique sequences, a C/A repeat variant in the *ARMS2* transcription regulator (indicated with a *blue box*) and an insertion/deletion variant downstream of exon 2 of *ARMS2* (indicated with a *red box*), were identified in a patient with AMD that carried the SNP, rs10490924. *B*, characteristic C/A mutations present in the *ARMS2* transcription regulatory region (*blue*, C/A variant; *red*, C to A substitution). *C*, the insertion/deletion mutations present in the *HTRA1* transcription regulatory region (*blue*, ARMS2 exon 2 region; *red*, point mutations). *D–G*, analysis of *ARMS2* transcription regulator activity using a luciferase assay system. *D*, four luciferase vectors were generated to analyze *ARMS2* transcription regulator activity: normal (1,000 bp), normal (600 bp), risk (1,000 bp), and risk (600 bp). The 1,000-bp sequence contained a C/T SNP in the upper 730-bp region from *ARMS2* exon 1. *ARMS2* transcription regulator activity detected in ARPE19 cells (*E*), RGC-5 cells (*F*), and 661W cells (*G*). *Error bars*, S.D. *H–K*, *HTRA1* transcription regulator activity detected in various retinal cell lines. *H*, schematic diagram of the *ARMS2-HTRA1* constructs used in the luciferase assays performed (*black line*, common regulator sequence; *blue line*, non-insertion/deletion regulator unique sequence; *red line*, insertion/deletion regulator unique sequence). Full-length *HTRA1* transcription regulator activity detected in ARPE19 cells (*I*), RGC5 cells (*, $p = 7.5 \times 10^{-6}$) (*J*), and 661W cells (**, $p = 1.07 \times 10^{-6}$) (*K*). *Error bars*, S.D. *EV*, empty vector; *NI*, non-insertion/deletion regulator; *I*, insertion/deletion regulator.

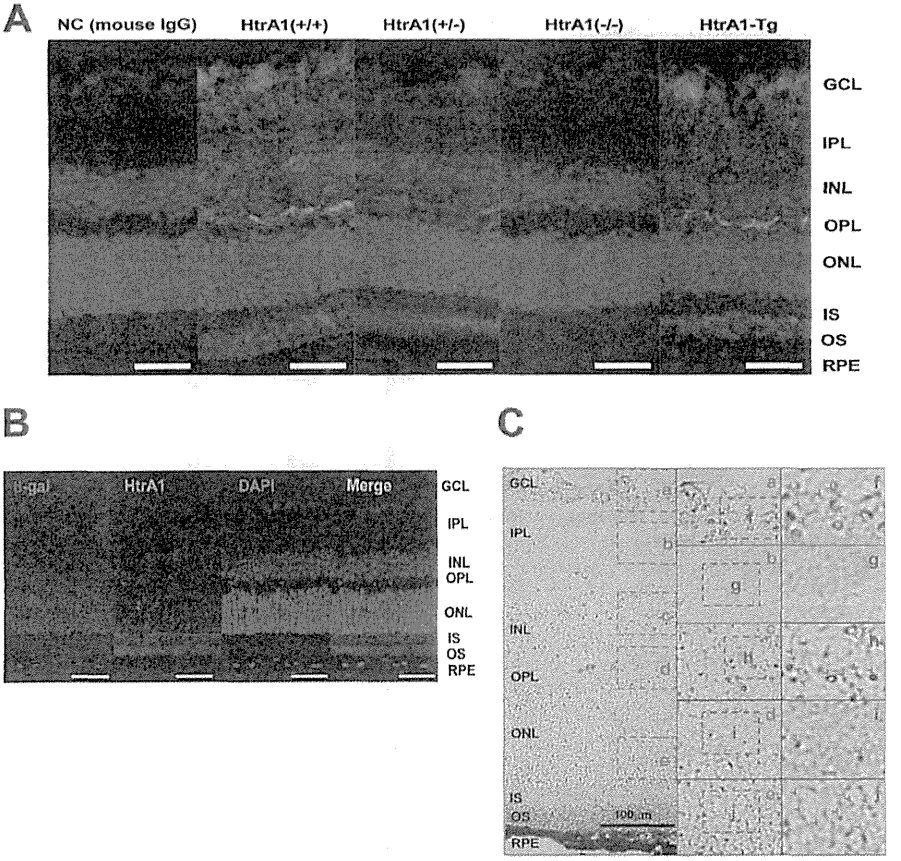

FIGURE 3. ***Htra1* transcription regulator activity and Htra1 protein expression in the mouse retina.** *A*, immunohistochemistry to detect HtrA1 expression in *HtrA1*$^{+/+}$, *HtrA1*$^{+/-}$, *HtrA1*$^{-/-}$, and *HtrA1-Tg* mouse retinas (*blue*, DAPI; *green*, HtrA1). *NC* (mouse IgG), staining control; *scale bars*, 100 μm. *B*, immunohistochemistry to detect HtrA1 expression in *HtrA1*$^{+/-}$ mouse retinas (*red*, β-galactosidase; green: HtrA1; *blue*, DAPI; *yellow*, merge). *Scale bars*, 100 μm. *C*, *in situ* hybridization to detect *HtrA1* expression in *HtrA1*$^{+/-}$ mouse retina tissues (*red arrowheads*, *HtrA1*; *blue arrowheads*, β-galactosidase). *Scale bars*, 100 μM. *OS*, outer segment; *IS*, inner segment; *ONL*, outer nuclear layer; *OPL*, outer plexiform layer; *INL*, inner nuclear layer; *IPL*, inner plexiform layer; *GCL*, ganglion cell layer.

HtrA1 expression was observed to localize to the photoreceptor cell layer (outer segment (*OS*) and inner segment (*IS*) in Fig. 3), the outer plexiform layer (*OPL*), and the ganglion cell layer (*GCL*). In contrast, HtrA1 expression in eye tissues from heterozygous *HtrA1* mice was mainly localized to the photoreceptor cell layer and the outer plexiform layer, whereas minor expression of HtrA1 was observed in the ganglion cell layer.

To localize *HtrA1* transcription regulator activity in the retina, a heterozygous *HtrA1* knock-out mouse construct that included β-galactosidase (β-gal) cDNA (*LacZ*) in place of exon 1 of *Htra1* was used. β-Gal protein was abundantly expressed in the outer nuclear layer (*ONL*), and lower levels of expression were observed in the RPE, the inner nuclear layer (*INL*), and the retinal ganglion cell layer (*GCL*) (Fig. 3*B*). In comparison, native HtrA1 protein was abundantly expressed in the OS and IS, with lower expression levels detected in the RPE, the outer plexiform layer (*OPL*), the inner plexiform layer (*IPL*), and the ganglion cell layer (Fig. 2*B*). Furthermore, abundant transcription of *HtrA1* mRNA was detected by *in situ* hybridization in retinal sections from a *HtrA1* heterozygous knock-out mouse (Fig. 3*C*). Taken together, these results suggest that *HtrA1* is transcribed mainly in the outer nuclear layer, outer plexiform layer, and ganglion cell layer, and then the protein product is transported to the photoreceptor layer.

Identification of Suppressing and Activating cis-Elements in the HTRA1 Regulatory Element—To analyze the mechanism of insertion/deletion function in the *HTRA1* regulatory region, both non-insertion/deletion (*1*, bp −4,320 to +1; *2*, bp −4,238 to +1; *3*, bp −4,022 to +1; *4*, bp −3,936 to +1; *5*, bp −3,777 to +1) and insertion/deletion (*6*, bp −3,936 to +1; *7*, bp −3,854 to +1; *8*, bp −3,788 to +1; *9*, bp −3,836 to −3,788 defect mutant) regions were cloned into a pGL4.10[*luc2*] luciferase assay vector (Fig. 4*A*). These cloned vectors were then transfected into 661W cells and were analyzed for *HTRA1* transcription regulator activity. The activity of the number 2 region (bp −4,320 to −4,239) non-insertion/deletion defect *HTRA1* transcription regulator was 1.8–2-fold higher than that of the number 1 region, and transcription regulator activity did not differ between the number 2, 3, and 4 variants (Fig. 4*B*). In contrast, the activity of the number 5 transcription regulator was 20–30% higher than that of the number 4 variant (Fig. 4*B*).

In addition, activity of the number 6 insertion/deletion type *HTRA1* transcription regulator was 2- and 3-fold higher than that of the number 1 non-insertion/deletion type transcription regulator in 661W cells (Figs. 1*K* and 4*C*). Furthermore, activity

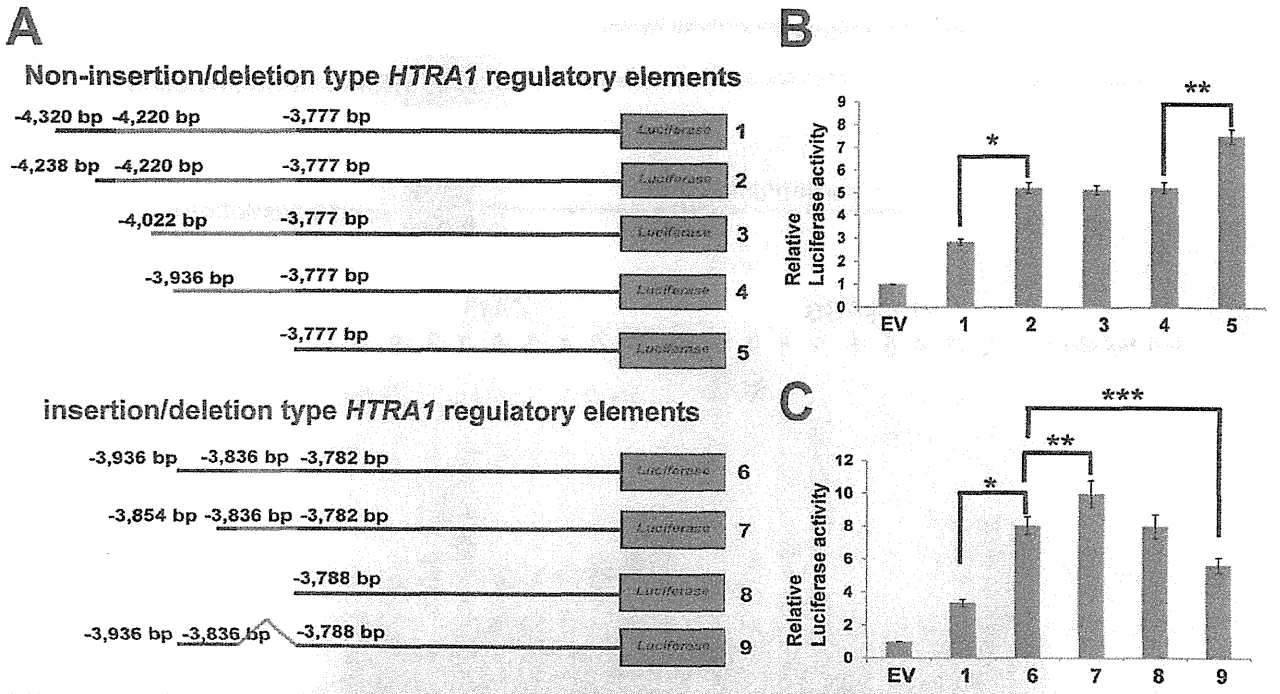

FIGURE 4. **Enhanced *HTRA1* transcription regulator activity is associated with the insertion/deletion variant in the photoreceptor cell line, 661W.** *A*, constructs used for luciferase assay analysis (*black line*, common sequence between both regulators; *blue line*, non-insertion/deletion regulator (443 bp); *red line*, insertion/deletion regulator (54 bp); *red boxes 1–5*, non-insertion/deletion regulator constructs; *green boxes 6–9*, insertion/deletion regulator constructs; *gray line 9*, insertion/deletion region). *B* and *C*, transcription regulator activity detected for the non-insertion/deletion and insertion/deletion *HTRA1* transcription regulator assayed (in *B*, *, $p = 1.05 \times 10^{-6}$; **, $p = 3.46 \times 10^{-5}$; in *C*, *, $p = 2.2 \times 10^{-6}$; **, $p = 0.0086$; ***, $p = 0.0062$). *EV*, empty vector; *error bars*, S.D.

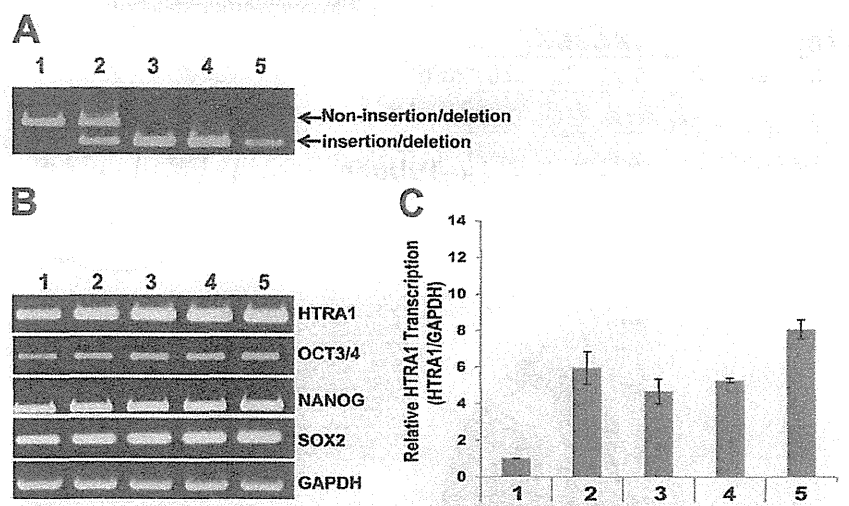

FIGURE 5. **HTRA1 transcription in human iPSCs derived from wet AMD patients.** *A*, genotyping of non-insertion/deletion *versus* insertion/deletion versions of the human *HTRA1* gene transcription regulatory region. *B*, detection of human iPSC marker genes by RT-PCR. Detection of GAPDH was used as an internal control. *C*, relative transcriptional level of *HTRA1* determined by quantitative RT-PCR for iPSCs derived from individuals with non-insertion/deletion (control) *versus* insertion/deletion (wet AMD) transcription regulators. *Sample 1*, 30-year-old non-AMD male; *sample 2*, 72-year-old wet AMD female; *sample 3*, 38-year-old non-AMD male; *sample 4*, 71-year-old non-AMD female; *sample 5*, 71-year-old wet AMD female. *Error bars*, S.D.

of the number 7 (bp −3,936 to −3,855 defect) region was 10% higher than that of the number 6 region, and activity of the number 8 (bp −3,936 to −3,789 defect) region was lower than that of the number 7 region (Fig. 4*C*). In addition, the activity of the number 9 (insertion/deletion defect) region was 10–20% lower than that of the number 6 insertion/deletion type transcription regulator (Fig. 4*C*). Taken together, these results suggest that both of the non-insertion/deletion type regions (including bp −4,320 to −4,239 and bp −3,936 to −3,778 bp) may be regulated by suppressor factors, whereas the insertion/deletion type region from bp −3,836 to −3,789 may bind an enhancer.

Endogenous HTRA1 Expression Is Enhanced by the Insertion/Deletion Type Regulatory Element in AMD Patient iPSCs—To determine the level of *HTRA1* expression in individuals with a non-insertion/deletion type regulatory element sequence,

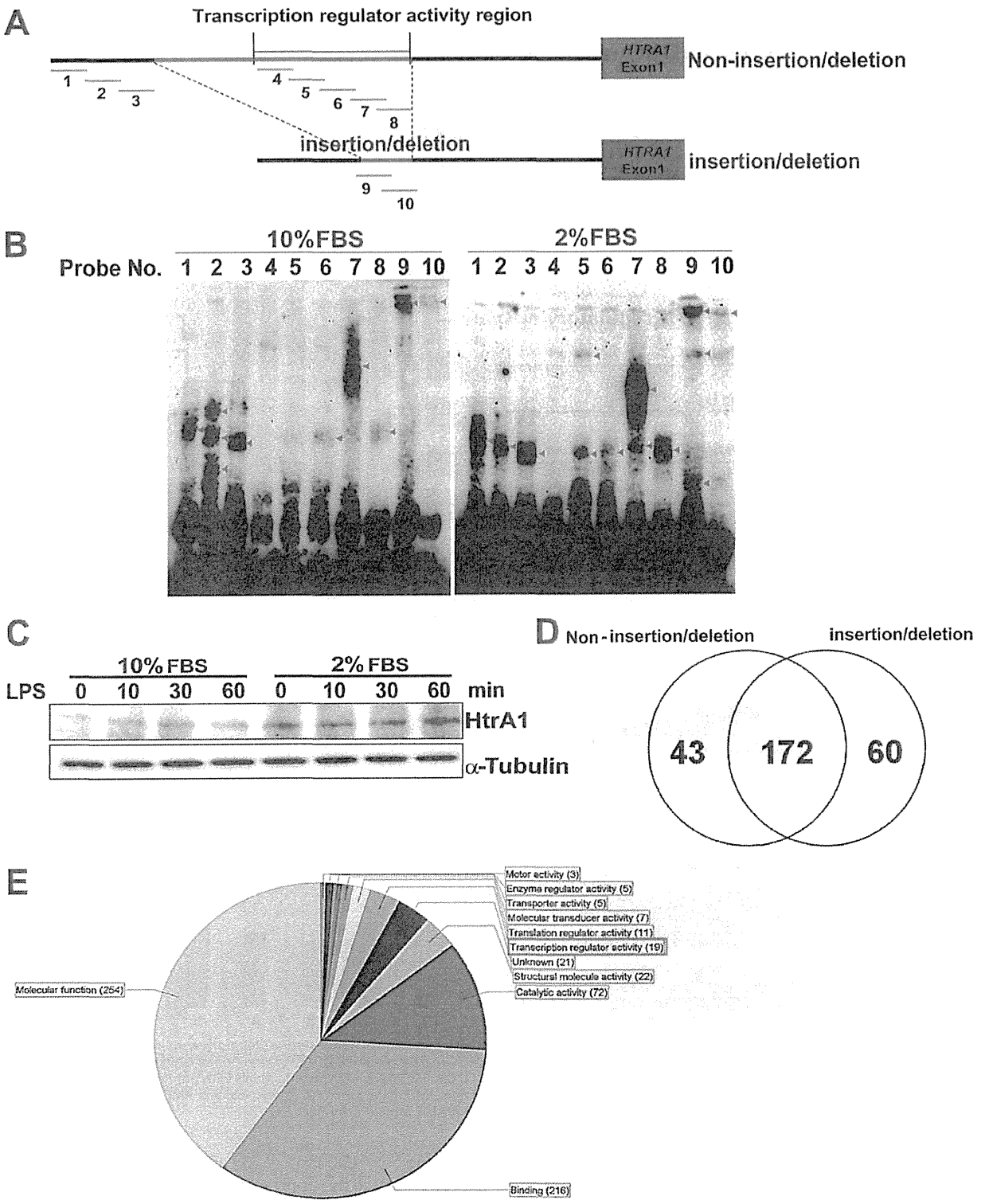

FIGURE 6. **Identification of the transcription factors binding to non-insertion/deletion and insertion/deletion regions of the *HTRA1* transcription regulators.** *A*, location of the double-stranded DNA probes, *1–10*, in the region upstream of the *HTRA1* coding region that were designed for EMSAs. Both non-insertion/deletion and insertion/deletion *HTRA1* transcription regulatory regions were targeted. *B*, EMSAs of probes 1–10 using nuclear extracts from 661W cells cultured in 2 and 10% FBS. *Red arrowheads*, detected signals. *C*, increased expression of HtrA1 was detected in Western blot assays performed following treatment of 661W cells with LPS (1 μg/ml, 0–60 min) using anti-mouse HtrA1 antibodies. Detection of α-tubulin was used as an internal control. *D*, a Venn diagram shows the number of proteins found to bind the non-insertion/deletion *versus* insertion/deletion regions of the *HTRA1* transcription regulator based on LC-MS/MS data. *E*, gene ontology term of non-insertion/deletion- and insertion/deletion-binding protein (categorized by molecular function).

iPSCs heterozygous and homozygous for the insertion/deletion type regulatory element sequence were subjected to genotyping. From both control and AMD patients, iPSCs were collected and categorized as having a non-insertion/deletion or insertion/deletion genotype (Fig. 5*A*). These cells were also assayed for expression of the iPSCs markers, OCT3/4, NANOG, and SOX2 (Fig. 5*B*), and levels of *HTRA1* mRNA were measured by RT-PCR and quantitative RT-PCR (Fig. 5, *B* and *C*). Individuals with heterozygous or homozygous *HTRA1* insertion/deletion type sequences showed an approximately 6- and 7-fold increase in *HTRA1* mRNA levels, respectively, compared with individuals having the non-insertion/deletion type sequence (Fig. 5*C*). In contrast, expression of *HTRA1* mRNA was not influenced by the heterozygous or homozygous state of the insertion/deletion type sequence.

Analysis of Regulatory Element-binding Proteins—To detect proteins that bind the *HTRA1* regulatory element, EMSAs were performed. Ten 3′-biotin-labeled double-stranded DNA probes were generated in order to assay the transcriptional activity of each region of the *HTRA1* regulatory element (Figs. 4 (*B* and *C*) and 6*A* and Table 3). In addition to the use of 661W nuclear extracts in these assays, extracts of 661W cells grown in 10% FBS *versus* 2% FBS were also assayed; the latter conditions were included based on the observation that HTRA1 family proteins are known to mediate various stress response signaling pathways (25–28). Thus, we tested 661W cell protein-probe binding activity in a cell-stressful environment. Protein-probe binding signals were detected for probes 1–3 and 6–10 (Fig. 6*A*) in the presence of nuclear extracts from normally cultured 661W cells (Fig. 6*B*, *left*). These results suggest that the binding pattern of the insertion/deletion sequence (included in probes 4–8) may differ greatly from that of the non-insertion/deletion type sequence (number 9 and 10 probes). When the culturing conditions for the 661W cells were changed from 10% to 2% FBS, this drastically altered the protein-probe binding signal pattern obtained (Fig. 6*B*, *right*). For example, a reduction in FBS concentration resulted in the loss of two of three signals for the number 2 probe, and it altered the probe-protein binding pattern of probes 5–9. Detection of HtrA1 expression further demonstrated that HtrA1 expression was enhanced in 661W cells following starvation stress (Fig. 6*C*). Signaling pathways involving the Toll-like receptor (TLR) family of proteins have been shown to be associated with AMD pathogenesis (29), and 661W cells are known to express TLR-4 (30). Therefore, HtrA1 expression was assayed in 661W cells following stimulation with a TLR-4 ligand, lipopolysaccharide (LPS). However, HtrA1 expression was unaffected by this stimulation (Fig. 6*C*).

To identify the proteins that bind the regulatory element region of *HTRA1*, both non-insertion/deletion and insertion/deletion sequence-binding factors were analyzed by LC-MS/MS. Non-insertion/deletion-binding protein samples were incubated with probes 4–8, whereas the insertion/deletion-binding protein samples were incubated with probes 9 and 10 (Fig. 6*A*). A total of 172 common binding proteins, 43 non-insertion/deletion probe-specific binding proteins, and 60 insertion/deletion probe-specific binding proteins were identified (Fig. 6*D*). Using Scaffold 4 software, 19 transcriptional regulator proteins were detected (according to gene ontology (see the Gene Ontology Consortium Web site)) (Fig. 6*E*). These 19 factors were then classified according to their binding sequence (Tables 4–6). Six non-insertion/deletion-binding probes were found to bind PURB, NFIC, RUNX2, PEBB, APEX1, and RBM14 proteins (Table 4), whereas three insertion/deletion-binding probes were found to bind LYRIC (lysine-rich CEACAM1 co-isolated) protein, MED4, and PHF2 (Table 5). Ten additional proteins were found to bind both the non-insertion/deletion and insertion/deletion probes: ROAA, SHOX2, CUX1, DDX5, DDX1, MED24, RBM39, JMY, TCP4, and DDX17 (Table 6). In combination, these results suggest that expression of *HtrA1* is influenced by factors that specifically bind this region and affect gene expression.

DISCUSSION

To the best of our knowledge, the present study provides the first detailed characterization of regulatory elements for *HTRA1* and the effect of insertion/deletion sequences associated with wet AMD. The insertion/deletion variant that exhibited complete association with the SNP, rs10490924, is the only major sequence change in this LD block and is likely to play a major role in disease onset. Moreover, the insertion/deletion variant in close proximity to *ARMS2* and *HTRA1* has been at the center of the discussion of whether one or both genes are involved in AMD (19, 24). In the present study, the *ARMS2* transcription regulator exhibited only marginal activity in each of the cell lines tested, whereas robust up-regulation of *HTRA1* transcription regulator activity was observed in iPSCs derived from AMD patients containing heterozygous or homozygous forms of the insertion/deletion. Up-regulation of *HTRA1* in the earliest stages of development is predicted to affect the entire body (31).

HTRA1 is known to be a TGF-β suppression factor, and some reports have suggested that HtrA1 is expressed in skeletal, brain, lung epithelium, heart, and skin tissues in fetal mice (31). Other reports have suggested that HTRA1 is involved in bone remodeling (*e.g.* RANK/RANKL signal-derived osteoclast bone absorption and osteoblast differentiation) (32) and oncogenesis in liver and lung cancers (33, 34). Thus, HTRA1 may play an important role in cell growth and differentiation, tissue and/or organ formation, and the onset of disorders. Correspondingly, a transgenic mouse with expression of mouse *HtrA1* driven by a chicken actin (CAG) promoter was used to establish a model for choroidal neovascularization, and this model exhibited a significant reduction in tolerance to smoking (23).

Detailed characterization of the transcription regulator activity that surrounds the *HTRA1* insertion/deletion sequence showed that suppressive regions are located between bp −4,320 and −4,239 and between bp −3,936 and −3,778 in the non-insertion/deletion sequence and between bp −3,936 and −3,854 for the insertion/deletion sequence. In addition, the insertion/deletion located between bp −3,836 and −3,783 exhibited transcription regulator activity unique to the insertion/deletion sequence (Fig. 4). An analysis of these results showed that the insertion/deletion variant interrupts a suppressor *cis*-element and replaces it with an activator, and this significantly alters *HTRA1* transcription in the photoreceptor.

TABLE 4

Non-insertion/deletion probe binding proteins

MS/MS view: identified proteins	Symbol	Molecular mass	Taxonomy	Biological regulation	Binding	Molecular function	Transcription regulator activity	Peptide hit score (non-indel)[a]	Peptide Hit Score (indel)
		kDa							
Transcriptional activator protein Pur-β	PURB	34	*M. musculus*	Regulation of transcription, DNA-dependent	Protein binding	Transcription factor activity	Transcription factor activity	3	0
Nuclear factor 1 C-type	NFIC	49	*M. musculus*	Regulation of transcription, DNA-dependent	Transcription factor activity	Transcription factor activity	Transcription factor activity	3	0
Runt-related transcription factor 2	RUNX2	66	*M. musculus*	Positive regulation of transcription from RNA polymerase II promoter	Protein binding	Transcription factor activity	Transcription factor activity	2	0
Core-binding factor subunit β	PEBB	22	*M. musculus*	Positive regulation of transcription from RNA polymerase II promoter	DNA binding	Transcription coactivator activity	Transcription coactivator activity	1	0
DNA-(apurinic or apyrimidinic site) lyase	APEX1	35	*M. musculus*	Cell redox homeostasis	Chromatin DNA binding	Transcription coactivator activity	Transcription coactivator activity	1	0
RNA-binding protein 14	RBM14	69	*M. musculus*	Regulation of transcription, DNA-dependent	Nucleic acid binding	Ligand-dependent nuclear receptor transcription coactivator activity	Ligand-dependent nuclear receptor transcription coactivator activity	1	0

[a] indel, insertion/deletion.

TABLE 5

Insertion/deletion probe binding proteins

MS/MS view: identified proteins	Symbol	Molecular mass	Taxonomy	Biological regulation	Binding	Molecular function	Transcription Regulator Activity	Peptide Hit Score (non-indel)[a]	Peptide Hit Score (indel)
		kDa							
Protein LYRIC	LYRIC	64	*M. musculus*	Positive regulation of NF-κB transcription factor activity	Nucleolus	Protein binding	Transcription coactivator activity	0	20
Mediator of RNA polymerase II transcription subunit 4	MED4	30	*M. musculus*	Androgen receptor signaling pathway	Thyroid hormone receptor binding	Transcription cofactor activity	Transcription cofactor activity	0	2
Lysine-specific demethylase PHF2	PHF2	121	*M. musculus*	Regulation of transcription, DNA-dependent	Methylated histone residue binding	Transcription coactivator activity	Transcription coactivator activity	0	1

[a] indel, insertion/deletion.

TABLE 6
Non-insertion/deletion-probe and insertion/deletion probe-binding proteins

MS/MS view: identified proteins	Symbol	Molecular mass	Taxonomy	Biological regulation	Binding	Molecular Function	Transcription Regulator Activity	Peptide hit score (non-indel)[a]	Peptide hit score (indel)
		kDa							
Heterogeneous nuclear ribonucleoprotein A/B	HNRPAB	31	*M. musculus*	Regulation of transcription, DNA-dependent	Nucleic acid binding	Transcription factor activity	Transcription factor activity	25	24
Short stature homeobox protein 2	SHOX2	35	*M. musculus*	Positive regulation of transcription from RNA polymerase II promoter	DNA binding	Transcription factor activity	Transcription factor activity	2	1
Homeobox protein cut-like 1	CUX1	166	*M. musculus*	Negative regulation of transcription from RNA polymerase II promoter	Chromatin binding	Transcription factor activity	Transcription factor activity	6	1
Probable ATP-dependent RNA helicase DDX5	DDX5	69	*M. musculus*	Regulation of alternative nuclear mRNA splicing, via spliceosome	Nucleic acid binding	Transcription coactivator activity	Transcription cofactor activity	14	36
ATP-dependent RNA helicase DDX1	DDX1	83	*M. musculus*	Regulation of transcription, DNA-dependent	Chromatin binding	Transcription cofactor activity	Transcription cofactor activity	28	12
Mediator of RNA polymerase II transcription subunit 24	MED24	110	*M. musculus*	Stem cell maintenance	Thyroid hormone receptor binding	Receptor activity	Transcription cofactor activity	1	1
RNA-binding protein 39	RBM39	59	*M. musculus*	Regulation of transcription, DNA-dependent	Nucleic acid binding	Transcription coactivator activity	Transcription coactivator activity	10	9
Junction-mediating and -regulatory protein	JMY	111	*M. musculus*	Positive regulation of transcription factor activity	Protein binding	Transcription coactivator activity	Transcription coactivator activity	1	1
Activated RNA polymerase II transcriptional coactivator p15	TCP4	14	*M. musculus*	Regulation of transcription from RNA polymerase II promoter	DNA binding	Transcription coactivator activity	Transcription coactivator activity	1	2
Probable ATP-dependent RNA helicase DDX17	DDX17	72	*M. musculus*	Regulation of transcription, DNA-dependent	Nucleic acid binding	Hydrolase activity	Transcription coactivator activity	1	1

[a] indel, insertion/deletion.

The EMSA and LC-MS/MS data also suggest that *HTRA1* regulatory element activity is regulated by a number of transcription factors (Fig. 6 and Tables 4–6).

When the proteins that bound the regulatory elements of the non-insertion/deletion and insertion/deletion sequences of *HTRA1* were analyzed using LC-MS/MS, LYRIC (also known as MTDH/AEG1) was a high hit score insertion/deletion-binding protein that was identified (Table 5). LYRIC is known to promote hepatocellular carcinoma and to activate the transcription factor, nuclear factor κ-B (NF-κB), and also has an effect on bone and brain metastasis (35–37). Regarding the latter, LYRIC may enhance the seeding of tumor cells at the target organ endothelium. LYRIC also contributes to HIF-1α-mediated angiogenesis (38), with HIF-1α playing an important role in the activation of VEGF signaling in response to oxidative stress (39). Recently, Oka *et al.* (25) reported that *HTRA1* gene expression is enhanced by oxidative stress. This result is consistent with the observation that AMD onset is associated with a variety of stresses, and stress response factors may play an important role.

Both common sequences (non-insertion/deletion (bp −4,320 to −4,220) and insertion/deletion (bp −3,936 to −3,836 bp)) and the insertion/deletion sequence (bp −3,836 to −3,782 bp) are partially associated with *ARMS2* exon 2, thereby indicating that this exon represents a protein-coding region and a *HTRA1* regulatory element region. Recent reports have suggested that both an increase in HTRA1 transcription and a decrease in ARMS2 transcription confer an increased risk of AMD (8). These insights suggest that *ARMS2* gene expression may be regulated by *HTRA1* transcription regulator activity via the *ARMS2* exon 2 region.

AMD pathogenesis and previous *HTRA1* experiments related to AMD have been performed and discussed in relation to the RPE (8, 16, 17). However, immunostaining of *HTRA1* in mouse retinas in the present study showed that the majority of transcription occurs in the photoreceptor cell layer (Fig. 3). This result was confirmed when higher levels of transcription from the *HTRA1* insertion/deletion regulator were observed in the photoreceptor cell line: 661W cells *versus* the RPE cells (Fig. 1, *I–K*). Photoreceptors are densely concentrated in the macula (40), which predicts that HTRA1 will also be concentrated in the macula. A recent report using transgenic mice overexpressing human HTRA1 in the RPE showed that PCV-like capillary structures could be observed in the choroid. Vierkotten *et al.* (17) also observed fragmentation of the elastic layer in Bruch's membrane, and Jones *et al.* (16) reported branching of choroidal vessels, polypoidal lesions, and severe degeneration of the elastic lamina or tunica media of choroidal vessels in the same model. When *HtrA1* expression was driven by the CAG promoter in a transgenic mouse model, an even more severe phenotype was induced compared with previous reports of AMD patient-like choroidal neovascularization (23). These results indicate that overexpression of HtrA1 alone can evoke choroidal vasculopathy or neovascularization, and they also provide supporting evidence for the association of the insertion/deletion variant of *HTRA1* regulatory element with wet AMD (7, 8).

REFERENCES

1. Fritsche, L. G., Chen, W., Schu, M., Yaspan, B. L., Yu, Y., Thorleifsson, G., Zack, D. J., Arakawa, S., Cipriani, V., Ripke, S., Igo, R. P., Jr., Buitendijk, G. H., Sim, X., Weeks, D. E., Guymer, R. H., Merriam, J. E., Francis, P. J., Hannum, G., Agarwal, A., Armbrecht, A. M., Audo, I., Aung, T., Barile, G. R., Benchaboune, M., Bird, A. C., Bishop, P. N., Branham, K. E., Brooks, M., Brucker, A. J., Cade, W. H., Cain, M. S., Campochiaro, P. A., Chan, C. C., Cheng, C. Y., Chew, E. Y., Chin, K. A., Chowers, I., Clayton, D. G., Cojocaru, R., Conley, Y. P., Cornes, B. K., Daly, M. J., Dhillon, B., Edwards, A. O., Evangelou, E., Fagerness, J., Ferreyra, H. A., Friedman, J. S., Geirsdottir, A., George, R. J., Gieger, C., Gupta, N., Hagstrom, S. A., Harding, S. P., Haritoglou, C., Heckenlively, J. R., Holz, F. G., Hughes, G., Ioannidis, J. P., Ishibashi, T., Joseph, P., Jun, G., Kamatani, Y., Katsanis, N., C, N. K., Khan, J. C., Kim, I. K., Kiyohara, Y., Klein, B. E., Klein, R., Kovach, J. L., Kozak, I., Lee, C. J., Lee, K. E., Lichtner, P., Lotery, A. J., Meitinger, T., Mitchell, P., Mohand-Said, S., Moore, A. T., Morgan, D. J., Morrison, M. A., Myers, C. E., Naj, A. C., Nakamura, Y., Okada, Y., Orlin, A., Ortube, M. C., Othman, M. I., Pappas, C., Park, K. H., Pauer, G. J., Peachey, N. S., Poch, O., Priya, R. R., Reynolds, R., Richardson, A. J., Ripp, R., Rudolph, G., Ryu, E., Sahel, J. A., Schaumberg, D. A., Scholl, H. P., Schwartz, S. G., Scott, W. K., Shahid, H., Sigurdsson, H., Silvestri, G., Sivakumaran, T. A., Smith, R. T., Sobrin, L., Souied, E. H., Stambolian, D. E., Stefansson, H., Sturgill-Short, G. M., Takahashi, A., Tosakulwong, N., Truitt, B. J., Tsironi, E. E., Uitterlinden, A. G., van Duijn, C. M., Vijaya, L., Vingerling, J. R., Vithana, E. N., Webster, A. R., Wichmann, H. E., Winkler, T. W., Wong, T. Y., Wright, A. F., Zelenika, D., Zhang, M., Zhao, L., Zhang, K., Klein, M. L., Hageman, G. S., Lathrop, G. M., Stefansson, K., Allikmets, R., Baird, P. N., Gorin, M. B., Wang, J. J., Klaver, C. C., Seddon, J. M., Pericak-Vance, M. A., Iyengar, S. K., Yates, J. R., Swaroop, A., Weber, B. H., Kubo, M., Deangelis, M. M., Leveillard, T., Thorsteinsdottir, U., Haines, J. L., Farrer, L. A., Heid, I. M., and Abecasis, G. R. (2013) Seven new loci associated with age-related macular degeneration. *Nat. Genet.* 10.1038/ng.2578
2. Klein, R. J., Zeiss, C., Chew, E. Y., Tsai, J. Y., Sackler, R. S., Haynes, C., Henning, A. K., SanGiovanni, J. P., Mane, S. M., Mayne, S. T., Bracken, M. B., Ferris, F. L., Ott, J., Barnstable, C., and Hoh, J. (2005) Complement factor H polymorphism in age-related macular degeneration. *Science* **308,** 385–389
3. Hageman, G. S., Anderson, D. H., Johnson, L. V., Hancox, L. S., Taiber, A. J., Hardisty, L. I., Hageman, J. L., Stockman, H. A., Borchardt, J. D., Gehrs, K. M., Smith, R. J., Silvestri, G., Russell, S. R., Klaver, C. C., Barbazetto, I., Chang, S., Yannuzzi, L. A., Barile, G. R., Merriam, J. C., Smith, R. T., Olsh, A. K., Bergeron, J., Zernant, J., Merriam, J. E., Gold, B., Dean, M., and Allikmets, R. (2005) A common haplotype in the complement regulatory gene factor H (HF1/CFH) predisposes individuals to age-related macular degeneration. *Proc. Natl. Acad. Sci. U.S.A.* **102,** 7227–7232
4. Okamoto, H., Umeda, S., Obazawa, M., Minami, M., Noda, T., Mizota, A., Honda, M., Tanaka, M., Koyama, R., Takagi, I., Sakamoto, Y., Saito, Y., Miyake, Y., and Iwata, T. (2006) Complement factor H polymorphisms in Japanese population with age-related macular degeneration. *Mol. Vis.* **12,** 156–158
5. Kondo, N., Honda, S., Ishibashi, K., Tsukahara, Y., and Negi, A. (2007) LOC387715/HTRA1 variants in polypoidal choroidal vasculopathy and age-related macular degeneration in a Japanese population. *Am. J. Ophthalmol.* **144,** 608–612
6. Goto, A., Akahori, M., Okamoto, H., Minami, M., Terauchi, N., Haruhata, Y., Obazawa, M., Noda, T., Honda, M., Mizota, A., Tanaka, M., Hayashi, T., Tanito, M., Ogata, N., and Iwata, T. (2009) Genetic analysis of typical wet-type age-related macular degeneration and polypoidal choroidal vasculopathy in Japanese population. *J. Ocul. Biol. Dis. Infor.* **2,** 164–175
7. Fritsche, L. G., Loenhardt, T., Janssen, A., Fisher, S. A., Rivera, A., Keilhauer, C. N., and Weber, B. H. (2008) Age-related macular degeneration is associated with an unstable ARMS2 (LOC387715) mRNA. *Nat. Genet.* **40,** 892–896
8. Yang, Z., Tong, Z., Chen, Y., Zeng, J., Lu, F., Sun, X., Zhao, C., Wang, K., Davey, L., Chen, H., London, N., Muramatsu, D., Salasar, F., Carmona, R., Kasuga, D., Wang, X., Bedell, M., Dixie, M., Zhao, P., Yang, R., Gibbs, D., Liu, X., Li, Y., Li, C., Li, Y., Campochiaro, B., Constantine, R., Zack, D. J., Campochiaro, P., Fu, Y., Li, D. Y., Katsanis, N., and Zhang, K. (2010) Genetic and functional dissection of HTRA1 and LOC387715 in age-related macular degeneration. *PLoS Genet.* **6,** e1000836
9. Kanda, A., Chen, W., Othman, M., Branham, K. E., Brooks, M., Khanna, R., He, S., Lyons, R., Abecasis, G. R., and Swaroop, A. (2007) A variant of mitochondrial protein LOC387715/ARMS2, not HTRA1, is strongly associated with age-related macular degeneration. *Proc. Natl. Acad. Sci. U.S.A.* **104,** 16227–16232
10. Kortvely, E., Hauck, S. M., Duetsch, G., Gloeckner, C. J., Kremmer, E., Alge-Priglinger, C. S., Deeg, C. A., and Ueffing, M. (2010) ARMS2 is a constituent of the extracellular matrix providing a link between familial and sporadic age-related macular degenerations. *Invest. Ophthalmol. Vis. Sci.* **51,** 79–88
11. Shiga, A., Nozaki, H., Yokoseki, A., Nihonmatsu, M., Kawata, H., Kato, T., Koyama, A., Arima, K., Ikeda, M., Katada, S., Toyoshima, Y., Takahashi, H., Tanaka, A., Nakano, I., Ikeuchi, T., Nishizawa, M., and Onodera, O. (2011) Cerebral small-vessel disease protein HTRA1 controls the amount of TGF-β1 via cleavage of proTGF-β1. *Hum. Mol. Genet.* **20,** 1800–1810
12. Zhang, L., Lim, S. L., Du, H., Zhang, M., Kozak, I., Hannum, G., Wang, X., Ouyang, H., Hughes, G., Zhao, L., Zhu, X., Lee, C., Su, Z., Zhou, X., Shaw, R., Geum, D., Wei, X., Zhu, J., Ideker, T., Oka, C., Wang, N., Yang, Z., Shaw, P. X., and Zhang, K. (2012) High temperature requirement factor A1 (HTRA1) gene regulates angiogenesis through transforming growth factor-β family member growth differentiation factor 6. *J. Biol. Chem.* **287,** 1520–1526
13. Jiang, J., Huang, L., Yu, W., Wu, X., Zhou, P., and Li, X. (2012) Overexpression of HTRA1 leads to down-regulation of fibronectin and functional changes in RF/6A cells and HUVECs. *PLoS One* **7,** e46115
14. Ferrer-Vaquer, A., Maurey, P., Werzowa, J., Firnberg, N., Leibbrandt, A., and Neubüser, A. (2008) Expression and regulation of HTRA1 during chick and early mouse development. *Dev. Dyn.* **237,** 1893–1900
15. Chien, J., Ota, T., Aletti, G., Shridhar, R., Boccellino, M., Quagliuolo, L., Baldi, A., and Shridhar, V. (2009) Serine protease HtrA1 associates with microtubules and inhibits cell migration. *Mol. Cell. Biol.* **29,** 4177–4187
16. Jones, A., Kumar, S., Zhang, N., Tong, Z., Yang, J. H., Watt, C., Anderson, J., Amrita, Fillerup, H., McCloskey, M., Luo, L., Yang, Z., Ambati, B., Marc, R., Oka, C., Zhang, K., and Fu, Y. (2011) Increased expression of multifunctional serine protease, HTRA1, in retinal pigment epithelium induces polypoidal choroidal vasculopathy in mice. *Proc. Natl. Acad. Sci. U.S.A.* **108,** 14578–14583
17. Vierkotten, S., Muether, P. S., and Fauser, S. (2011) Overexpression of HTRA1 leads to ultrastructural changes in the elastic layer of Bruch's membrane via cleavage of extracellular matrix components. *PLoS One* **6,** e22959
18. Hara, K., Shiga, A., Fukutake, T., Nozaki, H., Miyashita, A., Yokoseki, A., Kawata, H., Koyama, A., Arima, K., Takahashi, T., Ikeda, M., Shiota, H., Tamura, M., Shimoe, Y., Hirayama, M., Arisato, T., Yanagawa, S., Tanaka, A., Nakano, I., Ikeda, S., Yoshida, Y., Yamamoto, T., Ikeuchi, T., Kuwano, R., Nishizawa, M., Tsuji, S., and Onodera, O. (2009) Association of HTRA1 mutations and familial ischemic cerebral small-vessel disease. *N. Engl. J. Med.* **360,** 1729–1739
19. Dewan, A., Liu, M., Hartman, S., Zhang, S. S., Liu, D. T., Zhao, C., Tam, P. O., Chan, W. M., Lam, D. S., Snyder, M., Barnstable, C., Pang, C. P., and Hoh, J. (2006) HTRA1 promoter polymorphism in wet age-related macular degeneration. *Science* **314,** 989–992
20. Seddon, J. M., Ajani, U. A., and Mitchell, B. D. (1997) Familial aggregation of age-related maculopathy. *Am. J. Ophthalmol.* **123,** 199–206
21. Seki, T., Yuasa, S., Oda, M., Egashira, T., Yae, K., Kusumoto, D., Nakata, H., Tohyama, S., Hashimoto, H., Kodaira, M., Okada, Y., Seimiya, H., Fusaki, N., Hasegawa, M., and Fukuda, K. (2010) Generation of induced pluripotent stem cells from human terminally differentiated circulating T cells. *Cell Stem Cell* **7,** 11–14
22. Minegishi, Y., Iejima, D., Kobayashi, H., Chi, Z. L., Kawase, K., Yamamoto, T., Seki, T., Yuasa, S., Fukuda, K., and Iwata, T. (2013) Enhanced optineurin E50K-TBK1 interaction evokes protein insolubility and initiates familial primary open-angle glaucoma. *Hum. Mol. Genet.* **22,** 3559–3567
23. Nakayama, M., Iejima, D., Akahori, M., Kamei, J., Goto, A., and Iwata, T. (2014) Overexpression of HtrA1 and exposure to mainstream cigarette

smoke leads to choroidal neovascularization and subretinal deposits in aged mice. *Invest. Ophthalmol. Vis. Sci.* **55,** 6514–6523
24. Yang, Z., Camp, N. J., Sun, H., Tong, Z., Gibbs, D., Cameron, D. J., Chen, H., Zhao, Y., Pearson, E., Li, X., Chien, J., Dewan, A., Harmon, J., Bernstein, P. S., Shridhar, V., Zabriskie, N. A., Hoh, J., Howes, K., and Zhang, K. (2006) A variant of the HTRA1 gene increases susceptibility to age-related macular degeneration. *Science* **314,** 992–993
25. Supanji, Shimomachi, M., Hasan, M. Z., Kawaichi, M., and Oka, C. (2013) HtrA1 is induced by oxidative stress and enhances cell senescence through p38 MAPK pathway. *Exp. Eye Res.* **112,** 79–92
26. Hansen, G., and Hilgenfeld, R. (2013) Architecture and regulation of HtrA-family proteins involved in protein quality control and stress response. *Cell Mol. Life Sci.* **70,** 761–775
27. Gray, C. W., Ward, R. V., Karran, E., Turconi, S., Rowles, A., Viglienghi, D., Southan, C., Barton, A., Fantom, K. G., West, A., Savopoulos, J., Hassan, N. J., Clinkenbeard, H., Hanning, C., Amegadzie, B., Davis, J. B., Dingwall, C., Livi, G. P., and Creasy, C. L. (2000) Characterization of human HtrA2, a novel serine protease involved in the mammalian cellular stress response. *Eur. J. Biochem.* **267,** 5699–5710
28. Foucaud-Scheunemann, C., and Poquet, I. (2003) HtrA is a key factor in the response to specific stress conditions in *Lactococcus lactis*. *FEMS Microbiol. Lett.* **224,** 53–59
29. Kleinman, M. E., Kaneko, H., Cho, W. G., Dridi, S., Fowler, B. J., Blandford, A. D., Albuquerque, R. J., Hirano, Y., Terasaki, H., Kondo, M., Fujita, T., Ambati, B. K., Tarallo, V., Gelfand, B. D., Bogdanovich, S., Baffi, J. Z., and Ambati, J. (2012) Short-interfering RNAs induce retinal degeneration via TLR3 and IRF3. *Mol. Ther.* **20,** 101–108
30. Tu, Z., Portillo, J. A., Howell, S., Bu, H., Subauste, C. S., Al-Ubaidi, M. R., Pearlman, E., and Lin, F. (2011) Photoreceptor cells constitutively express functional TLR4. *J. Neuroimmunol.* **230,** 183–187
31. Oka, C., Tsujimoto, R., Kajikawa, M., Koshiba-Takeuchi, K., Ina, J., Yano, M., Tsuchiya, A., Ueta, Y., Soma, A., Kanda, H., Matsumoto, M., and Kawaichi, M. (2004) HtrA1 serine protease inhibits signaling mediated by Tgfβ family proteins. *Development* **131,** 1041–1053
32. Wu, X., Chim, S. M., Kuek, V., Lim, B. S., Chow, S. T., Zhao, J., Yang, S., Rosen, V., Tickner, J., and Xu, J. (2014) HtrA1 is upregulated during RANKL-induced osteoclastogenesis, and negatively regulates osteoblast differentiation and BMP2-induced Smad1/5/8, ERK and p38 phosphorylation. *FEBS Lett.* **588,** 143–150
33. Zhu, F., Jin, L., Luo, T. P., Luo, G. H., Tan, Y., and Qin, X. H. (2010) Serine protease HtrA1 expression in human hepatocellular carcinoma. *Hepatobiliary Pancreat. Dis. Int.* **9,** 508–512
34. Xu, Y., Jiang, Z., Zhang, Z., Sun, N., Zhang, M., Xie, J., Li, T., Hou, Y., and Wu, D. (2013) HtrA1 downregulation induces cisplatin resistance in lung adenocarcinoma by promoting cancer stem cell-like properties. *J. Cell. Biochem.* **115,** 1112–1121
35. Ash, S. C., Yang, D. Q., and Britt, D. E. (2008) LYRIC/AEG-1 overexpression modulates BCCIPα protein levels in prostate tumor cells. *Biochem. Biophys. Res. Commun.* **371,** 333–338
36. Robertson, C. L., Srivastava, J., Siddiq, A., Gredler, R., Emdad, L., Rajasekaran, D., Akiel, M., Shen, X. N., Guo, C., Giashuddin, S., Wang, X. Y., Ghosh, S., Subler, M. A., Windle, J. J., Fisher, P. B., and Sarkar, D. (2014) Genetic deletion of AEG-1 prevents hepatocarcinogenesis. *Cancer Res.* **74,** 6184–6193
37. Huang, Y., and Li, L. P. (2014) Progress of cancer research on astrocyte elevated gene-1/metadherin (review). *Oncol. Lett.* **8,** 493–501
38. Noch, E., Bookland, M., and Khalili, K. (2011) Astrocyte-elevated gene-1 (AEG-1) induction by hypoxia and glucose deprivation in glioblastoma. *Cancer Biol. Ther.* **11,** 32–39
39. Domigan, C. K., and Iruela-Arispe, M. L. (2014) Stealing VEGF from thy neighbor. *Cell* **159,** 473–474
40. Li, K. Y., Tiruveedhula, P., and Roorda, A. (2010) Intersubject variability of foveal cone photoreceptor density in relation to eye length. *Invest. Ophthalmol. Vis. Sci.* **51,** 6858–6867

Overexpression of *HtrA1* and Exposure to Mainstream Cigarette Smoke Leads to Choroidal Neovascularization and Subretinal Deposits in Aged Mice

Mao Nakayama,[1] Daisuke Iejima,[1] Masakazu Akahori,[1] Junzo Kamei,[2] Asako Goto,[1] and Takeshi Iwata[1]

[1]Division of Molecular and Cellular Biology, National Institute of Sensory Organs, National Hospital Organization Tokyo Medical Center, Tokyo, Japan
[2]Department of Pathophysiology and Therapeutics, Hoshi University, Tokyo, Japan

Correspondence: Takeshi Iwata, Division of Molecular and Cellular Biology, National Institute of Sensory Organs, National Hospital Organization Tokyo MedicalCenter, 2-5-1 Higashigaoka, Meguro-ku, Tokyo 152-8902, Japan; iwatatakeshi@kankakuki.go.jp.

MN and DI are joint first authors.

MN and DI contributed equally to the work presented here and should therefore be regarded as equivalent authors.

Submitted: March 27, 2014
Accepted: September 2, 2014

Citation: Nakayama M, Iejima D, Akahori M, Kamei J, Goto A, Iwata T. Overexpression of *HtrA1* and exposure to mainstream cigarette smoke leads to choroidal neovascularization and subretinal deposits in aged mice. *Invest Ophthalmol Vis Sci.* 2014;55:6514–6523. DOI:10.1167/iovs.14-14453

Purpose. We determined the function of ARMS2 and HtrA1 in the choroid and retina using transgenic (Tg) mice and evaluated the effects of mainstream cigarette smoke on these mice.

Methods. The chicken actin promoter (CAG) was used to drive mouse *HtrA1*, human *ARMS2*, and *ARMS2 (A69S)* expression in the entire body of a mouse for one year. Fundus observations were performed with a Spectralis HRA+ optical coherence tomograph (OCT). Eyes were sectioned, stained with hematoxylin and eosin (H&E), and analyzed with immunohistochemistry. Mice were exposed to cigarette smoke for 30 min/d, 5 d/wk for 12 weeks using a mainstream smoking chamber (INH06-CIGR02A, MIPS). After 12 weeks, fundus observations and pathological analyses were performed.

Results. Approximately 18.2% of 12-month-old *HtrA1* Tg mice exhibited choroidal neovascularization (CNV) by OCT and positive immunostaining with anti-CD31 and anti-fibronectin antibodies. Furthermore, elastic van Gieson (EVG) staining showed Bruch's membrane damage in *HtrA1* Tg mice. No retinal changes were observed in *ARMS2* and *ARMS2 (A69S)* Tg mice. A total of 12 weeks of exposure to mainstream cigarette smoke led to CNV rates of 7.7% for wild type (Wt) mice and 20% for *HtrA1* Tg mice, but had no effect on *ARMS2* Tg mice. In addition, abnormal deposits were observed between photoreceptor cells and the RPE in an *HtrA1* Tg mouse exposed to mainstream cigarette smoke.

Conclusions. The *HtrA1* overexpression and mainstream cigarette smoke can independently lead to CNV. The *HtrA1* gene is a strong risk factor for wet AMD, but not all of the *HtrA1* Tg mice developed CNV, suggesting that CNV development depends on multiple risk factors.

Keywords: age-related macular degeneration, HtrA1, ARMS2, CNV, transgenic mouse

Age-related macular degeneration (AMD) is the leading cause of severe irreversible central vision loss and blindness in individuals over 65 years of age in developed countries.[1,2] This condition is separated into two types based on pathological characteristics. In dry AMD, drusen deposits are observed initially between the retinal pigment epithelium (RPE) and Bruch's membrane (BM) and there is a gradual progression to geographic atrophy, whereas in wet AMD, vision loss occurs by choroidal neovascularization (CNV) or polypoidal choroidal vasculopathy (PCV) of the macula.[3] Caucasian AMD patients predominantly exhibit geographic atrophy, while Japanese AMD patients present with CNV or PCV with few or no drusen.[4,5] Genetic and environmental factors are believed to be involved in the onset of AMD.[6] A recent genome-wide association study (GWAS) revealed more than 30 AMD susceptibility gene loci.[4,7–9] Single nucleotide polymorphisms (SNPs) in complement factor H (*CFH*), such as rs800292 (I62V) and rs1061170 (T402H) on chromosome 1q32, have been associated with AMD in Caucasians,[4,7,10] but not with AMD in Chinese or Japanese patients.[7,11–16] Another locus strongly associated with AMD is on chromosome 10q26, which is the chromosome where *ARMS2* (age-related maculopathy susceptibility) and *HtrA1* (high-temperature requirement factor A1) also are located.[10] Our previous GWAS study also showed strong associations between SNPs rs10490924, rs800292, and rs2241394 at the same locus, and wet AMD and PCV in Japanese patients. Within the linkage disequilibrium (LD) of these SNPs, a large insertion/deletion (indel) sequence variation was found downstream of *ARMS2* at the promoter region of *HTRA1*.[4,17]

It has been controversial whether this indel variant is responsible for the instability of *ARMS2* mRNA or for the upregulation of *HTRA1* transcription.[10,18–22] We showed that the indel in the *HTRA1* promoter upregulates transcription in a photoreceptor-derived cell line, but not in the RPE (data not shown; Iejima et al., submitted for publication). The presence and localization of ARMS2 also has been controversial.[19,23,24] A previous study found that ARMS2 localized to the mitochondria, and that ARMS2 and ARMS2 (A69S) were found in extracellular fractions.[23] Another study showed that ARMS2 was distributed primarily in the cytosol rather than in the outer membrane of mitochondria.[24] In addition, a study suggested that ARMS2 is

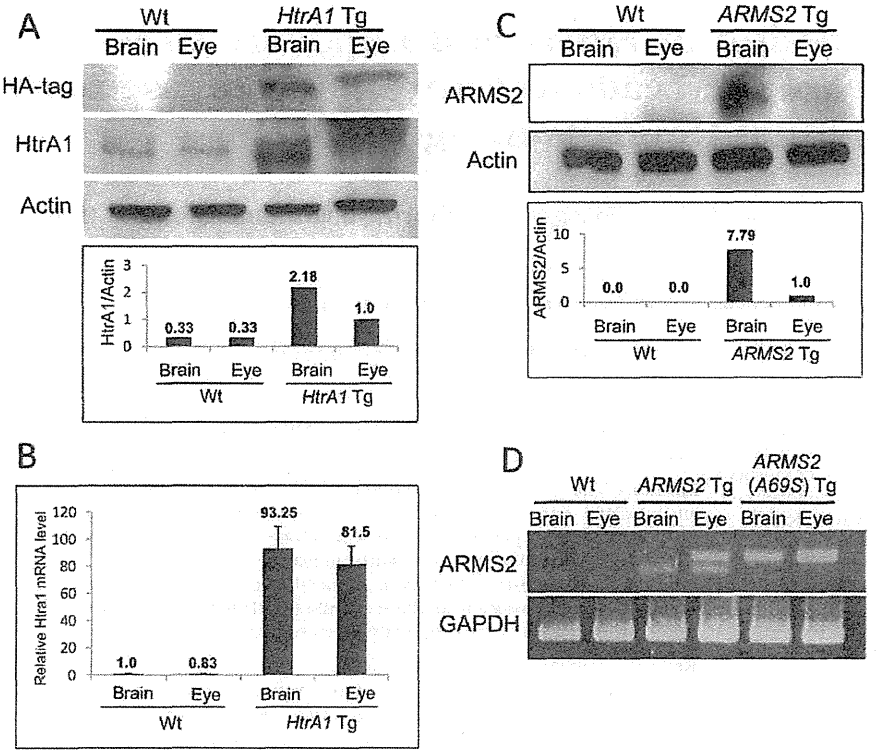

FIGURE 1. Ubiquitous expression of mouse *HtrA1*, human *ARMS2*, or *ARMS2 (A69S)* using the CAG promoter in mice. (**A**) Western blot analysis of mouse *HtrA1* expression in the brains and eyes of mice. *HtrA1* expression was detected in brains and eyes using an anti-HtrA1 and anti-HA antibody. The relative intensity of a band for the transgenic eye tissue toward a housekeeper was taken as 1.0. The HtrA1 protein level was significantly higher in the *HtrA1* Tg mouse eye than in the Wt mouse eye. (**B**) Quantitative real-time PCR determination of *HtrA1* mRNA levels from total RNA isolated from brains and eyes of Wt and *HtrA1* Tg mice. The Wt mouse brain was assigned a value of 1.0. The *HtrA1* mRNA level in an *HtrA1* Tg mouse was significantly higher than in a Wt mouse. (**C**) Western blot analysis of human *ARMS2* expression in the mouse brain and eye. The ARMS2 protein was detected in transgenic mouse using an anti-ARMS2 antibody. (**D**) Analysis of *ARMS2* mRNA expression in *ARMS2* and *ARMS2 (A69S)* Tg mice by PCR amplification. The *ARMS2* mRNA was detected in the brain and eye.

not synthesized in individuals homozygous for the indel variant; thus, ARMS2 may be the AMD risk-factor within this locus.[23] Furthermore, SNPs in *ARMS2* that change alanine to serine at codon 69 (A69S) may function as surrogate markers for the downstream indel. The *ARMS2* gene consists of two exons, which encode a poorly characterized 107 amino acid protein with no similarities to known protein motifs.[23] In this study, *ARMS2* and *ARMS2 (A69S)* were expressed ubiquitously in mice to observe their effects on eye development and aging.

Environmental risk factors also have been associated with AMD. Smoking is a major environmental risk factor that increases disease onset approximately 2- to 20-fold.[7,25–31] Cigarette smoke, which contains chemical toxins, may affect metabolic processes in the RPE by repressing the release of antioxidants and by altering choroidal blood flow.[7] A recent report showed that smoking damaged mitochondrial DNA, but not nuclear DNA, and increased degradation processes in the RPE.[32] A number of studies found an independent association between smoking and the risk of advanced AMD with no susceptibility genes acting as modifiers, except *ARMS2*.[7,33] In mouse models, exposure to cigarette smoke led to oxidative damage with structural degradation of the RPE and BM.[34] Smoke-related oxidants also led to the formation of subretinal deposits.[35]

Based on the observation that *HtrA1* expression was higher in fibroblasts isolated from AMD patients than in fibroblasts from healthy subjects,[18] we created human *ARMS2*, human *ARMS2 (A69S)*, and *HtrA1* transgenic (Tg) mice. We used the chicken actin promoter (CAG) to ubiquitously express these genes. We characterized pathological changes during aging and compared them to those observed in human AMD patients. Pathological changes were observed for up to 12 months after birth by fundus observation, fluorescein angiography (FA), indocyanine green angiography (IA), and optical coherence tomography (OCT). Because upregulation of susceptible genes and mainstream cigarette smoke are two essential risk factors for AMD, Tg mice also were exposed to mainstream cigarette smoke to evaluate genetic and environmental risk factors for disease progression.

METHODS

Construction of *ARMS2*, *ARMS2 (A69S)*, and *HtrA1* Tg Mice

The *ARMS2* cDNA was PCR amplified (PrimeSTAR HS DNA Polymerase; TaKaRa Bio, Otsu, Japan) from a human retina cDNA library (Clontech Laboratories, Inc., Mountain View, CA, USA) and ligated into pCAGGS, an expression vector containing a CAG promoter and an HA-tag at the C-terminus. The *HtrA1* cDNA was PCR amplified from a mouse brain cDNA library and ligated into pCAGGS, an expression vector containing a CAG promoter and an HA-tag at the N-terminus.

Investigative Ophthalmology & Visual Science

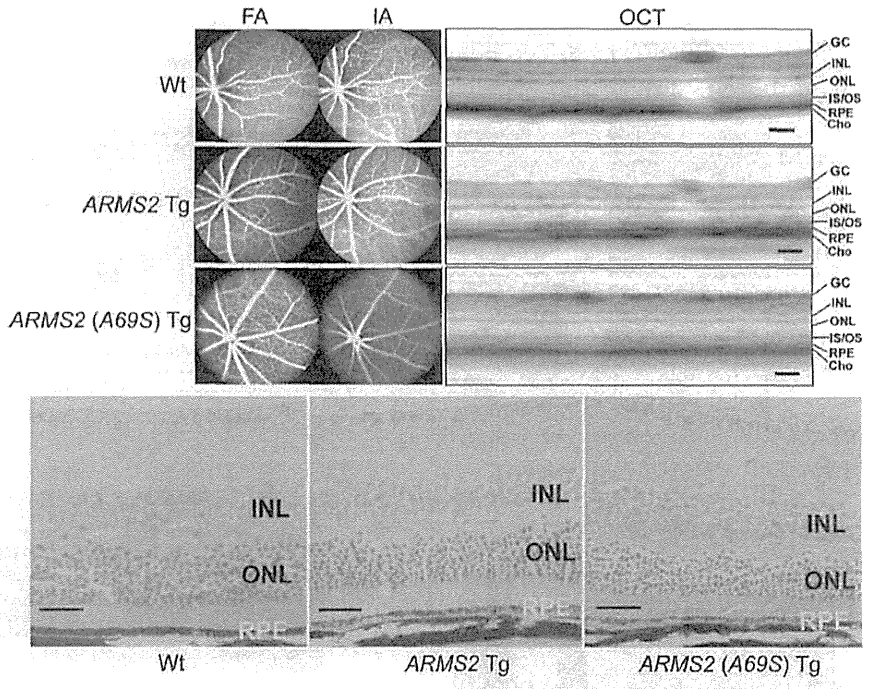

FIGURE 2. No retinal abnormalities in 12-month-old *ARMS2* Tg and *ARMS2 (A69S)* Tg mice by fundus observation. The *ARMS2* Tg and *ARMS2 (A69S)* Tg mice showed no retinal abnormalities at 1 year by fundus observation (*scale bars*: 200 μm) and H&E staining (×40 magnification; *scale bars*: 20 μm).

Linearized inserts were injected into pronuclear stage BDF1/C57BL6N embryos to create the Tg mice (PhoenixBio Co., Hiroshima, Japan).

The *ARMS2* and *ARMS2 (A69S)* Tg mice were screened by PCR (PrimeSTAR HS DNA Polymerase; TaKaRa Bio) using the forward primer 5′-ATGCTGCGCCTATACCCAGG-3′ and the reverse primer 5′-AGTGTCAGGTGGTGCTGAGG-3′ followed by Sanger sequencing (BigDye Terminator v3.1 Cycle Sequencing Kit; Invitrogen, Carlsbad, CA, USA). The *HtrA1* Tg mice were screened by PCR using the forward primer 5′-GAGCCTCTGC TAACCATGTTGA-3′ and the reverse primer 5′-CAGCAGTAG CAAAGACAGGAGC-3′ followed by Sanger sequencing.

Nine Tg lines with 2 to 11 copies of mouse *HtrA1* cDNA were generated. The Tg line with 11 copies was selected and bred with C57BL6N for seven generations before using the mice for experiments. All experiments were approved by the National Hospital Organization Experimental Animal Committee and the Hoshi University Experimental Animal Committee. All mice experiments were performed in accordance with the Association for Research in Vision and Ophthalmology (ARVO) Statement for the Use of Animals in Ophthalmic and Vision Research.

Western Blotting

Proteins from mouse brain and eye tissue were extracted in ice-cold TNE buffer containing protease and phosphatase inhibitors (1697498; Hoffmann-La Roche, Basel, Switzerland). Protein concentrations were determined using the BCA assay kit (Pierce; Thermo Fisher Scientific, Waltham, MA, USA). Equal amounts of protein (25 μg/lane) were separated by 7.5% SDS-PAGE and transferred to polyvinylidine fluoride (PVDF) membranes (Trans-Blot Turbo; Bio-Rad Laboratories, Inc., Hercules, CA, USA) for Western blotting with anti-mouse HtrA1 (1:100 dilution; ab38611; Abcam, Cambridge, UK), anti-HA (1:1000 dilution; 631207; Clontech Laboratories, Inc.), anti-human ARMS2 (1:1000 dilution; ABN160; Millipore Corporation, Billerica, MA, USA), and anti-actin (1:1000 dilution; MAB1501; Millipore Corporation) antibodies. The FluorChem Western Blot Imaging Station (ChemiDoc XRS+; Bio-Rad Laboratories, Inc.) was used to capture the images. The pixel value for each protein band was determined and normalized using image analysis software (Image Lab; Bio-Rad Laboratories, Inc.).

Quantitative RT-PCR (qRT-PCR)

Total RNA was isolated from the eyes and brains of Tg and wild type (Wt) mice using an RNeasy Mini kit (Qiagen, Venlo, The Netherlands) according to the manufacturer's instructions, and aliquots were reverse-transcribed to generate single-stranded cDNA (High Capacity cDNA Reverse Transcription Kit; Life Technologies, Carlsbad, CA, USA). The qRT-PCR was performed using an ABI STEP-One Real-time PCR system (Life Technologies) and a TaqMan probe (mouse *HtrA1*) according to the manufacturer's instructions. All reactions were run in triplicate using human glyceraldehyde-3-phosphate dehydrogenase (*GAPDH*) as the internal control and ΔCt normalization.

RNA Preparation and PCR Amplification in *ARMS2 (A69S)* Tg Mice

Total RNA was isolated from mice brains and eyeballs using TRIzol Reagent (Life Technologies). Single-stranded oligo (dT)-primed cDNA was generated using Superscript II Reverse Transcriptase (Life Technologies). The *ARMS2* was PCR amplified (PrimeSTAR HS DNA Polymerase, TaKaRa Bio) using

Investigative Ophthalmology & Visual Science

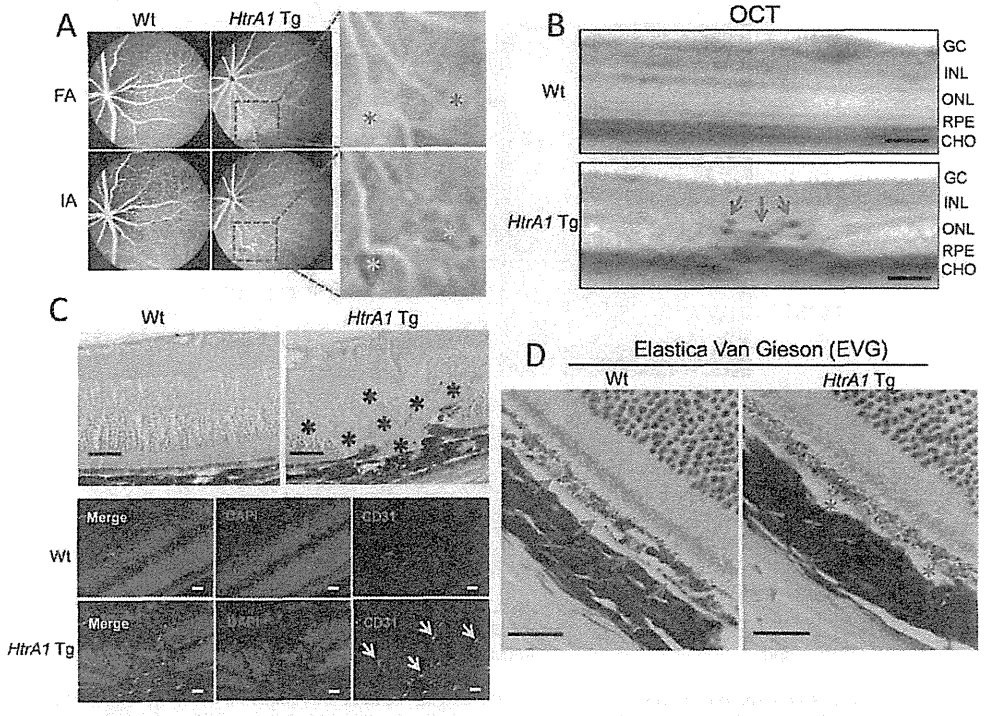

FIGURE 3. The 12-month-old *HtrA1* Tg mice developed CNV. (**A**) The *HtrA1* Tg mice showed hyperfluorescent lesions by FA (*red asterisks*) and networks of abnormally branching vessels by IA (*yellow asterisks*). (**B**) The CNV was observed in the choroid and retina by OCT (*red arrowheads*; *scale bar*: 200 μm). (**C**) The H&E staining of the FA and IA lesions on the retinal sections showed radial CNV spreading from the choroid through the RPE into the retina (*black asterisks*; ×40 magnification; *scale bars*: 20 μm). The endothelial cell marker CD31 was stained (*green*) in a radial CNV (*white arrowheads*; *scale bars*: 20 μm). Nuclei were stained with DAPI (*blue*). (**D**) The EVG staining of BM (*red arrowheads*). The *HtrA1* Tg mice displayed ruptures and deficiencies in the BM (*red asterisks*; ×100 magnification; *scale bars*: 10 μm).

the forward primer 5′-GCCAACTGGAGCTTCTCATC-3′ and the reverse primer 5′-GATTTCACCAGCTGCACAGA-3′. Mouse *GAPDH* (450 base pairs [bp]) was used as the control (forward primer, 5′-GGGGAGCCAAAAGGGTCATCATCT-3′; reverse primer, 5′-CGACGCCTGCTTCACCACCTTCTT-3′).

Angiography Observation and Retinal OCT of CNV

For in vivo imaging, 12-month-old *ARMS2*, *ARMS2 (A69S)*, and *HtrA1* Tg mice were anesthetized by injecting ketamine (Daiichi Sankyo, Chuo, Japan) at 0.002 mL/g body weight into their abdominal cavities. Pupils were dilated with 5 mg/mL Tropicamide (Santen Pharmaceutical Co., Ltd., Osaka, Japan). Fundus examinations were performed using a small animal retinal-imaging microscope (Micron III; Phoenix Research Products, Candler, NC, USA). The FA, IA, and OCT studies were performed using a retinal-imaging device (Spectralis HRA+OCT, Heidelberg Engineering, Heidelberg, Germany). Retinal vasculature imaging by FA and choroidal vasculature imaging by IA were performed simultaneously. Morphological changes, and angiographs of mouse retinas and choroids were visualized by OCT using a 3.2-mm diameter polymethylmethacrylate (PMMA) mouse contact lens (Ocular Instruments, Inc., Bellevue, WA, USA) to adjust the light path. Mice were tail-injected with 100 μL fluorescein sodium (100 mg/mL, 1:10 dilution; Alcon, Fort Worth, TX, USA) immediately before imaging and with 100 μL indocyanine green (25 mg/3 mL, 1:10 dilution; Santen Pharmaceutical Co.) 5 minutes before imaging.

Histology and Immunohistochemistry

Mice were anesthetized by injecting 1 mL pentobarbital (64.8 mg/mL, Kyoritsu Seiyaku, Tokyo, Japan) into their abdominal cavities and their hearts were cut open to sacrifice the mice. The eyes were removed quickly and immersed in a fixative solution containing 5% formaldehyde overnight at 4°C. The eyes were embedded in paraffin and sectioned at 5-μm thickness. After deparaffinization and rehydration, sections were hematoxylin and eosin (H&E) stained and elastica van Gieson (EVG) stained (Elastic Statin kit HT25A, Sigma-Aldrich Corp., St. Louis, MO, USA). The H&E- and EVG-stained images were collected using a Nikon Eclipse light microscope (Nikon Corporation, Tokyo, Japan). After deparaffinization and rehydration, eye sections were treated with Target Retrieval Solution (DakoCytomation, Glostrup, Denmark) at 120°C for 10 minutes. They then were incubated with blocking solution for 1 hour followed by overnight incubation with primary anti-CD31 antibody (1:50 dilution; Santa Cruz Biotechnology, Inc., Santa Cruz, CA, USA) in PBS containing 2% BSA at 4°C. Sections were washed with PBS three times and then were incubated with Alexa Fluor 488 conjugated rabbit anti-mouse IgG (1:500 dilution; Life Technologies) and 4′6-diamidino-2-phenylindole (DAPI) for nuclear staining (1:1000 dilution; Wako Chemicals GmbH, Neuss, Germany) for 1 hour at room temperature. Slides were mounted with Ultramount Aqueous Permanent Mounting Medium (DakoCytomation) and viewed with a confocal fluorescence laser microscope (LSM 700, Carl Zeiss Meditech, Jena, Germany).

Investigative Ophthalmology & Visual Science

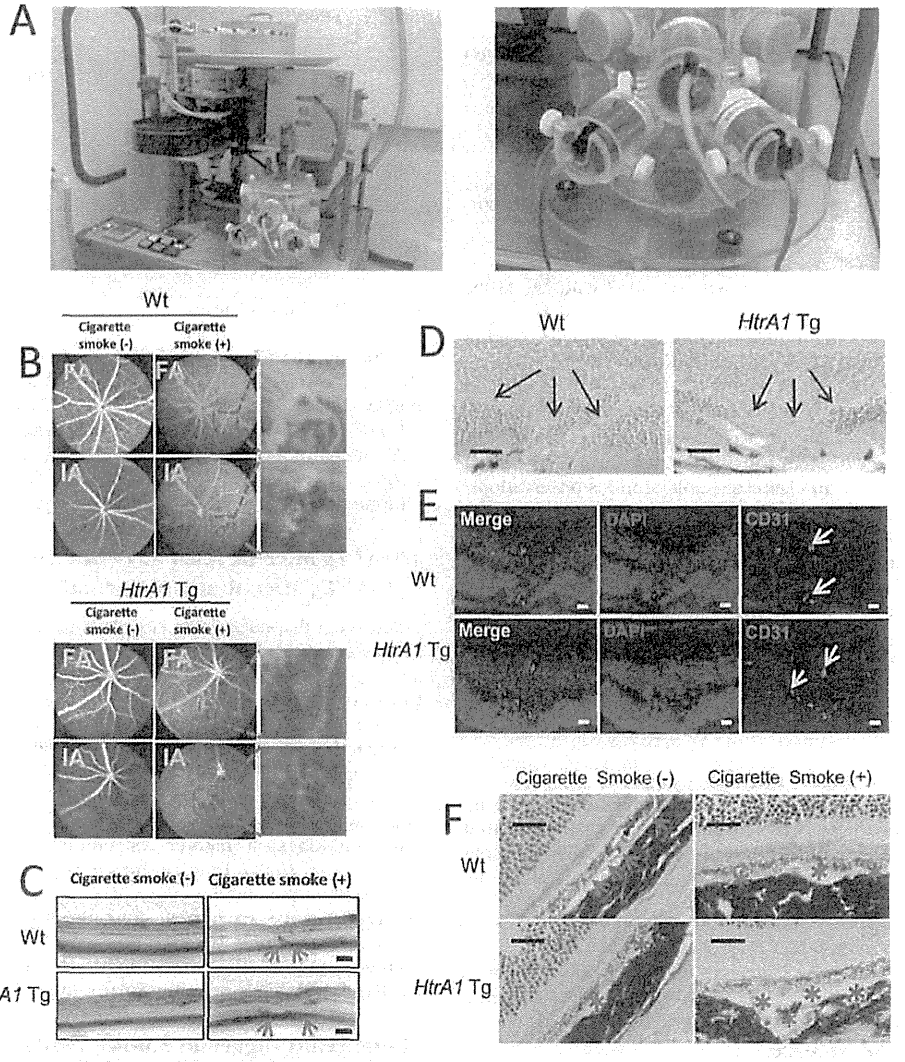

FIGURE 4. Effect of cigarette smoke on CNV in 12-month-old Wt and *HtrA1* Tg mice. (**A**) The 12-month-old Wt and *HtrA1* Tg mice were exposed to mainstream cigarette smoke (diluted 1:7 with compressed air) from Natural America Spirit cigarettes (*left*). Mice were placed into smoke chambers (*right*) for 30 min/d, 5 d/wk for 12 weeks. The smoke flow rate was 0.35 L/min. (**B**) After 12 weeks of exposure to cigarette smoke, hyperfluorescent lesions were observed by FA and networks of abnormally branching vessels were observed by IA in Wt and *HtrA1* Tg mice (*red boxes*). The networks of abnormally branching vessels spread further and were more clearly visible in *HtrA1* Tg mice than in Wt mice. (**C**) The OCT of FA and IA lesions in Wt and *HtrA1* Tg mice, respectively. Photoreceptor cells were thinner. *HtrA1* Tg mice displayed more severe retinal abnormalities than Wt mice (*red arrowheads*; *scale bars*: 200 μm). (**D**) Retinal sections stained with H&E displayed radial CNV formations (*black arrowheads*; ×40 magnification; *scale bars*: 20 μm). (**E**) The endothelial cell marker CD31 was stained (*green*) within a radial CNV formation (*white arrowheads*; *scale bars*: 20 μm). Nuclei were stained with DAPI (*blue*). (**F**) The EVG staining showed ruptures or deficiencies in the BMs of Wt mice, but *HtrA1* Tg mice showed more BM damage after exposure to mainstream cigarette smoke (*red asterisks*, ×100 magnification; *scale bars*: 10 μm).

Transmission Electron Microscopy (TEM)

Mice eyes were dissected and immersed in a fixative containing 2% formaldehyde overnight at 4°C. Tissue samples for TEM were fixed in phosphate-buffered 2% glutaraldehyde (EM grade; Electron Microscopy Science, Hatfield, PA, USA) and postfixed in 2% osmium tetroxide (Crystal; Heraeus Chemicals, Port Elizabeth, South Africa) for 3 hours in an ice bath. Specimens then were dehydrated in graded ethanol (Nakarai Tesque, Inc., Nakagyo-ku, Japan) and embedded in epoxy resin (TAAB Laboratories, Berkshire, UK). Ultrathin sections were cut at 70 to 80 nm by an ultramicrotome with diamond knives (Diatome Ltd., Biel, Switzerland) and mounted on 200 mesh copper grids. Ultrathin sections were stained with uranyl acetate for 10 minutes and with a lead staining solution for 5 minutes; stained sections were submitted for TEM (JEM-2000EX and JEM-1200; JEOL Ltd., Akashima, Japan) to the Hanaichi Ultrastructure Research Institute (Aichi, Japan).

Exposure to Mainstream Cigarette Smoke

The 12-month-old *ARMS2*, *ARMS2 (A69S)*, *HtrA1* Tg, and Wt mice with normal fundi were exposed to mainstream cigarette smoke for 30 min/d, 5 d/wk for 12 weeks using a mainstream

Investigative Ophthalmology & Visual Science

Table 1. CNV in Wt, *HtrA1*, *ARMS2*, and *ARMS2 (A69S)* Tg Mice

	Wt	*HtrA1* Tg	*ARMS2* Tg	*ARMS2 (A69S)* Tg
N of mice	40	22	20	20
N of mice with CNV	0	4	0	0
CNV rate, %	0	18.2	0	0

Approximately 18.2% of *HtrA1* Tg mice displayed CNV. $P < 0.005$, Fisher's exact test.

smoking chamber for small animals (INH06-CIGR02A, MIPS, see Fig. 4A). Natural American Spirit cigarettes, which contain 12 mg of tar and 1.5 mg of nicotine per cigarette, were used in this experiment. Mainstream cigarette smoke was diluted 1:7 with compressed air. Mice were placed in the chamber and exposed to smoke at a flow rate of 0.35 L/min. Control mice were placed in the chamber without cigarette smoke to evaluate the effect of stress on the retina. After 12 weeks of exposure to mainstream cigarette smoke, fundus observations, FA, IA, and OCT were performed. Mice then were sacrificed for eye sectioning followed by H&E staining and immunostaining. All experiments were approved by the National Hospital Organization Experimental Animal Committee and the Hoshi University Experimental Animal Committee. All mice experiments were performed in accordance with the ARVO Statement for the Use of Animals in Ophthalmic and Vision Research.

Statistics

Data of qRT-PCR were analyzed using the StatView 5.0 statistical software package (SAS Institute, Inc., Chicago, IL, USA). Continuous data between two groups were compared using Student's *t*-test. All pathological data were analyzed using Fisher's exact test. *P* values < 0.05 were considered statistically significant.

Results

Ubiquitous Expression of Mouse *HtrA1* and Human *ARMS2* in Mice

The CAG was used to create Tg mice that overexpress mouse *HtrA1*, human *ARMS2*, or *ARMS2 (A69S)*. An HA-tag at the C-terminus of recombinant HtrA1 was used to detect expression of recombinant Htra1 in the brains and eyes of mice by western blotting.

Levels of HtrA1 in the brains and eyes of mice were studied by Western blotting. The HtrA1 levels were 6.6- and 3.0-fold higher in *HtrA1* Tg mice brains and eyes, respectively, than in Wt mice brains and eyes (Fig. 1A). In addition, *HtrA1* mRNA levels were higher in *HtrA1* Tg mice than in Wt mice. The brains and eyes of *HtrA1* Tg mice had 93.2- and 98.2-fold higher *HtrA1* mRNA levels, respectively, compared to Wt (Fig. 1B).

Human ARMS2 was detected in the brains and eyes of *ARMS2* Tg mice (Fig. 1C). The *ARMS2* and *ARMS2 (A69S)* mRNAs were detected in the brains and eyes of *ARMS2* and *ARMS2 (A69S)* Tg mice (Fig. 1D). Fundus observations and H&E stains of eye sections showed that *ARMS2* and *ARMS2 (A69S)* Tg mice had no abnormalities in their retinas and choroids up to 12 months after birth (Fig. 2).

Table 2. Effects of Mainstream Cigarette Smoke on CNV and Subretinal Deposits in Wt and *HtrA1* Tg Mice

	Wt	*HtrA1* Tg	*ARMS2* Tg
N of mice exposed to smoke, 30 min/d, 5 d/wk, 12 wks	13	10	9
N of mice with CNV	1	2	0
CNV rate, %	7.7	20	0

There was no significant difference in the CNV rates of *HtrA1* Tg and Wt mice. $P > 0.5$, Fisher's exact test.

Table 3. Effect of Cigarette Smoke on Subretinal Deposits in *HtrA1* Tg Mice

	Wt	*HtrA1* Tg	*ARMS2* Tg
N of mice exposed to smoke, 30 min/d, 5 d/wk, 12 wks	13	10	9
N of mice with subretinal deposits	0	1	0
Subretinal deposits rate, %	0	10	0

Of *HtrA1* Tg mice, 10% had subretinal deposits ($P > 0.05$, Fisher's exact test).

HtrA1 Tg Mice Develop CNV but *ARMS2* and *ARMS2 (A69S)* Tg Mice Remain Normal

Fluorescein diapedesis was observed in *HtrA1* Tg mice fundi, suggesting the breakdown of the blood–retinal barrier (BRB) and aggravation of retinal vascular permeability. Lesions with low fluorescence were observed in *HtrA1* Tg mice choroids by IA and indicated the presence of networks of abnormally branched vessels (Fig. 3A). Additionally, radial capillary branching from the choroid through the RPE and into the retina was observed by OCT (Fig. 3B). Radial CNV formation was explored further by H&E staining and immunostaining with anti-CD31, a marker for endothelial cells (Fig. 3C). Furthermore, *HtrA1* Tg mice showed ruptures and deficiencies in BMs by EVG staining (Fig. 3D). Of the 22 12-month-old *HtrA1* Tg mice examined, four developed CNV (18.2%), compared to none of the 40 12-month-old Wt mice. In contrast, none of the 20 12-month old *ARMS2* and *ARMS2 (A69S)* Tg mice had any abnormal retinal changes (Table 1).

Mainstream Cigarette Smoke Leads to CNV in *HtrA1* Tg and Wt Mice

The *HtrA1* Tg, *ARMS2* Tg, and Wt mice were exposed to mainstream cigarette smoke as described in the Materials and Methods section. All mice used for this experiment were 12 months old. Two of 10 *HtrA1* Tg mice that were exposed to mainstream cigarette smoke developed CNV (Table 2), compared to none of the control group that was exposed to air (Table 4). The *HtrA1* Tg mice exposed to mainstream cigarette smoke displayed hyperfluorescent lesions by FA and lesions with low fluorescence by IA. Networks of abnormally branching vessels were observed in lesions with low fluorescence (Fig. 4B). The OCT images of the FA and IA lesions showed abnormal morphological changes in the choroid and

Table 4. No Retinal Changes Were Found in Wt, *HtrA1* Tg, and *ARMS2* Tg Mice Exposed to Air

	Wt	*HtrA1* Tg	*ARMS2* Tg
N of mice exposed to air, 30 min/d, 5 d/wk, 12 wks	10	10	10
N of mice with CNV	0	0	0
N of mice with subretinal deposits	0	0	0

Investigative Ophthalmology & Visual Science

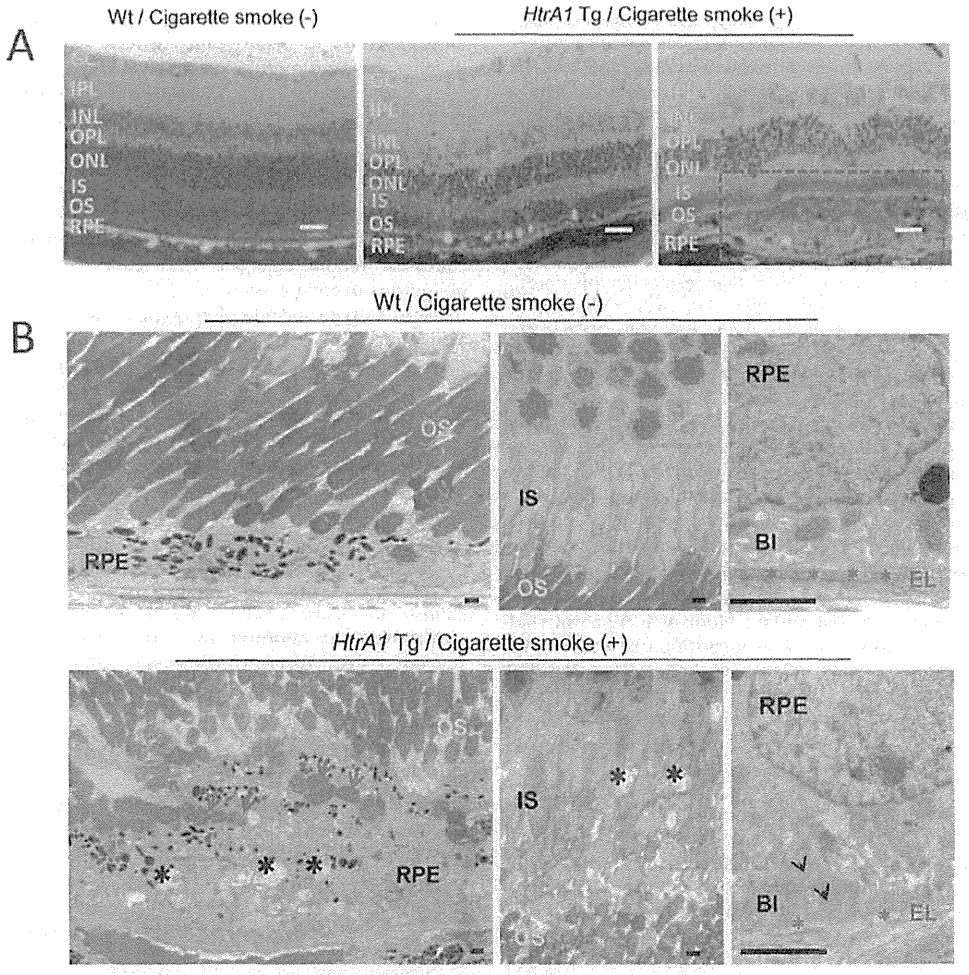

FIGURE 5. Effect of cigarette smoke on subretinal deposits in 12-month-old *HtrA1* Tg mice. (A) Retinal electron micrograph of an *HtrA1* Tg mouse exposed to smoke shows RPE degeneration with severe pigment loss and vacuolization (*red arrowheads*). Abnormal deposits were observed between photoreceptor cells and RPE cells in an *HtrA1* Tg mouse exposed to smoke (*red boxes*; ×20 magnification; *scale bars*: 20 μm). (B) Vacuolization (*black asterisks*) and the fragmented outer segment (*red arrowheads*) were observed in RPE (*lower left*). Photoreceptor cells were aligned in a disorderly manner and vacuolization occurred between and within the inner segment (*lower middle*, *black asterisks*). Basal infolding with thick subretinal deposits (*black arrowheads*) and a BM lacking elastic lamina (*red asterisks*) were observed (*lower right* photo). BI, basal infolding; EL, elastic lamina. *Scale bars*: 2 μm.

retinal layer (Fig. 4C). Radial CNV spreading from the choroid to the retina was observed by H&E staining and confirmed by immunostaining with anti-CD31 (Figs. 4D, 4E). The *HtrA1* Tg mice showed ruptures and deficiencies in BMs, but equivalent damage also was observed in Wt mice exposed to mainstream cigarette smoke (Fig. 4F). Our results showed that exposure to mainstream cigarette smoke triggered CNV, and the formation of CNV was independent of the level of HtrA1 expressed.

Accumulation of Subretinal Deposits in *HtrA1* Tg Mice Exposed to Mainstream Cigarette Smoke

A single *HtrA1* Tg mouse exposed to mainstream cigarette smoke for 12 weeks developed dense deposits in the subretinal space (Fig. 5A). Electron micrographs revealed RPE degeneration with severe pigment loss and abnormal deposits or vacuolization in the subretinal space of one *HtrA1* Tg mouse exposed to mainstream cigarette smoke (Fig. 5B). The molecular content of these deposits currently is under investigation. Although only one of 10 *HtrA1* Tg mice had subretinal deposits, no *ARMS2* Tg mice or Wt mice, with or without exposure to mainstream cigarette smoke, had any subretinal deposits (Table 3). Further, none of the *HtrA1* Tg mice exposed to air for 12 weeks had retinal degeneration (Table 4). Our results suggested that overexpression of HtrA1 combined with mainstream cigarette smoke can cause formation of abnormal subretinal deposits.

DISCUSSION

The *HTRA1* gene is a member of a family of serine proteases and is involved in the degradation of extracellular matrix (ECM) proteins, like fibronectin and aggrecan.[36,37] Mutations in this gene have been associated with hereditary cerebral small-vessel disease (CSVD).[6,38] Because *HtrA1* was found to be expressed similarly in mouse and human retinas,[39,40] we generated a mouse line that overexpressed mouse *HtrA1*

Investigative Ophthalmology & Visual Science

throughout the entire mouse body and observed CNV progression in aged mice. Wet AMD is characterized by CNV or PCV. The CNV results from the growth of new blood vessels from the choroid into the RPE and subretinal spaces, whereas PCV results from inner choroidal vessel abnormalities with intact basement membranes and collagenous fibers in the BM.[41,42] The BM depends on the adjacent RPE and choroidal cells, and is important for AMD development, particularly for CNV formation in wet AMD. Degradation of BM and upregulation of VEGF are risk factors for CNV.[43,44] Targeted expression of human *HtrA1* in the mouse RPE has led to the development of PCV, but not CNV.[41] Our results demonstrated, for the first time to our knowledge, that overexpression of mouse *HtrA1* in the entire mouse body can induce CNV. No drusen-like deposits at the basal RPE in *HtrA1* Tg mice were observed. Of the 22 12-month-old *HtrA1* Tg mice that we examined, four displayed CNV.

In AMD patients with CNV, the promoter region of *HTRA1* is highly associated with CNV. Risk variant 18 leads to a 2.7-fold mRNA increase in *HTRA1* in the RPE and is estimated to confer a population attributable risk of 49.3%. In our mouse model, an approximately 98.2-fold increase in *HtrA1* mRNA in the mouse eye (Fig. 1B) led to an attributed CNV risk of 18.2%. Our results suggested that the level of *HtrA1* expression may influence CNV progression and that other unknown environmental risk factors may influence the risk variant. None of 40 12-month-old Wt mice examined displayed CNV, suggesting that the level of *HtrA1* expression is more influential than aging. Previous studies have suggested that overexpression of *HtrA1* in the RPE can lead to an altered BM with fragmentation of the elastic lamina.[6,41] Our study also found ruptured or deficient BMs when *HtrA1* was overexpressed ubiquitously.

Cigarette smoke, which contains numerous potential oxidants, including nitric oxide, carbon monoxide, and many other toxic chemical moieties, is considered to be the environmental risk factor most strongly associated with early-stage AMD.[45] In human studies, cigarette smoking induces RPE abnormalities, such as geographic atrophy of the RPE and cell death from apoptosis, which also are changes associated with aging and early-stage AMD.[34,46,47] Mice exposed to chronic cigarette smoke develop evidence of oxidative damage, such as ultrastructural degeneration of the RPE and BM, as well as RPE apoptosis.[34] In our study, exposure to mainstream cigarette smoke enhanced the rates of CNV in *HtrA1* Tg mice and Wt mice. Two (20%) of 10 *HtrA1* Tg mice examined had radial CNV, compared to one (7.7%) of 13 Wt mice. The number of Tg mice, with and without CNV, at 12 months was extremely limited. Although the number of mice tested was low and although our results were statistically insignificant, we speculated that smoking does not significantly alter the occurrence of CNV.

In this study, *HtrA1* Tg mice exposed to cigarette smoke displayed RPE degeneration, severe pigment loss, vacuolization, and numerous wave-like morphological disorders in the outer nuclear layer of the retina, as well as abnormal deposits at the apical side of the RPE. Although the mechanisms of this retinal degeneration still are unknown, previous reports have shown that treatment with endogenous double-stranded RNAs (dsRNA) led to RPE loss and that activation of a receptor involved in innate immunity, Toll-Like receptor 3 (TLR3), affected retinal morphology.[48–50] A recent report showed that TLR3 activation led to a wave-like morphology in the outer nuclear retinal layer. This wave-like layer also was found to contain late apoptotic cells.[51] Of the 10 *HtrA1* Tg mice exposed to smoke that we examined, one displayed signs of RPE degeneration, including subretinal deposits similar to the advanced form of dry AMD. No RPE damage was found in Wt mice or in *HtrA1* Tg mice that were not exposed to smoke. Our results showed that overexpression of *HtrA1* combined with exposure to mainstream cigarette smoke leads to RPE degeneration and morphological changes in the retina.

A recent report showed that ARMS2 is a constituent of the ECM; this localization suggests that ARMS2 may be necessary for proper matrix function and may protect against drusen formation.[23] We examined 20 aged *ARMS2* Tg mice and 20 aged *ARMS2 (A69S)* Tg mice, but none displayed any retinal changes. Furthermore, nine of the 20 aged *ARMS2* Tg mice that were exposed to mainstream cigarette smoke showed no abnormal retinal changes. Our results demonstrated that ubiquitous overexpression of *ARMS2* or *ARMS2 (A69S)* does not lead to typical AMD phenotypes, such as drusen or CNV formation. We were unable to confirm whether ARMS2 protects against CNV formation induced by mainstream cigarette smoke.

In summary, aged mice that ubiquitously overexpress *HtrA1* develop CNV similar to human AMD patients. Exposure to mainstream cigarette smoke enhanced the CNV rate in *HtrA1* Tg and Wt mice. Furthermore, *HtrA1* Tg mice exposed to mainstream cigarette smoke developed subretinal deposits and a wave-like retinal morphology. Extended networks of branching vessels covering much of the retina were observed in *HtrA1* Tg mice, but not in *ARMS2* Tg or Wt mice exposed to mainstream cigarette smoke. Morphological changes also were observed in the photoreceptor layer of the CNV. Our study suggested that *HtrA1* overexpression alone is a strong risk factor for wet AMD, which is the predominant form of AMD in the Japanese population.

Acknowledgments

The authors thank Koichi Yanagisawa of JFC Sales Plan Co., Ltd. for use of the Spectralis HRA+OCT (Heidelberg Engineering) and for his technical assistance.

Supported by grants to by the Japanese Ministry of Health, Labor and Welfare (10103254 [TI]) and the Japan Society for the Promotion of Science (24592664 [MN], 23890258 [DI], and 22791704 [MA]).

Disclosure: **M. Nakayama**, None; **D. Iejima**, None; **M. Akahori**, None; **J. Kamei**, None; **A. Goto**, None; **T. Iwata**, None

References

1. Cousins SW, Espinosa-Heidmann DG, Miller DM, et al. Macrophage activation associated with chronic murine cytomegalovirus infection results in more severe experimental choroidal neovascularization. *PLoS Pathog.* 2012;8:e1002671.
2. Klein R, Klein BE, Jensen SC, Meuer SM. The five-year incidence and progression of age-related maculopathy: the Beaver Dam Eye Study. *Ophthalmology.* 1997;104:7–21.
3. Vingerling JR, Dielemans I, Hofman A, et al. The prevalence of age-related maculopathy in the Rotterdam Study. *Ophthalmology.* 1995;102:205–210.
4. Goto A, Akahori M, Okamoto H, et al. Genetic analysis of typical wet-type age-related macular degeneration and polypoidal choroidal vasculopathy in Japanese population. *J Ocul Biol Dis Infor.* 2009;2:164–175.
5. Maruko I, Iida T, Saito M, Nagayama D, Saito K. Clinical characteristics of exudative age-related macular degeneration in Japanese patients. *Am J Ophthalmol.* 2007;144:15–22.
6. Vierkotten S, Muether PS, Fauser S. Overexpression of HTRA1 leads to ultrastructural changes in the elastic layer of Bruch's membrane via cleavage of extracellular matrix components. *PLoS One.* 2011;6:e22959.